Title Ajay

ORIGINALITY REPORT

4%	3%	2%	%
SIMILARITY INDEX	INTERNET SOURCES	PUBLICATIONS	STUDENT PAPERS

PRIMARY SOURCES

1	Energy Efficiency in Process Technology, 1993. Publication	1%
2	digilib.library.usp.ac.fj Internet Source	1%
3	Senbin Yu, Rajesh Sadanandan, Xue-Song Bai. "Numerical studies of flame extinction and re-ignition behaviors in a novel, ultra-lean, non-premixed model GT burner using LES-ESF method", Fuel, 2020 Publication	1%
4	www.einsteincollege.ac.in Internet Source	1%
5	"Numerical Approaches to Combustion Modeling", American Institute of Aeronautics and Astronautics (AIAA), 1991 Publication	<1%
6	baixardoc.com Internet Source	<1%
7	mdpi-res.com Internet Source	<1%

8	1heart.nl Internet Source	<1 %
9	www.studyblue.com Internet Source	<1 %

Exclude quotes	On	Exclude matches	< 10 words
Exclude bibliography	On		

Spectral emissions from a swirl-stabilized and non-premixed methane/air flame

A project report submitted

in partial fulfillment for the award of the degree of

Bachelor of Technology

in

Aerospace Engineering

by

Ajay Daniel Pravin

Department of Aerospace Engineering

Indian Institute of Space Science and Technology

Thiruvananthapuram, India

January - May 2023

Certificate

This is to certify that the project report titled ***Spectral emissions from a swirl-stabilized and non-premixed methane/air flame*** submitted by **Ajay Daniel Pravin**, to the Indian Institute of Space Science and Technology, Thiruvananthapuram, in partial fulfillment for the award of the degree of **Bachelor of Technology** is a bona fide record of the original work carried out by him/her under my supervision. The contents of this project report, in full or in parts, have not been submitted to any other Institute or University for the award of any degree or diploma.

Dr. Rajesh Sadanandan
Professor
Department of Aerospace Engineering
Indian Institute of Space Science and Technology
Thiruvananthapuram

Place: Thiruvananthapuram
Date: January - May 2023

Declaration

I declare that this project report titled ***Spectral emissions from a swirl-stabilized and non-premixed methane/air flame*** submitted in partial fulfillment for the award of the degree of **Bachelor of Technology** in **Aerospace Engineering** is a record of the original work carried out by me under the supervision of **Dr. Rajesh Sadanandan**, and has not formed the basis for the award of any degree, diploma, associateship, fellowship, or other titles in this or any other Institution or University of higher learning. In keeping with the ethical practice in reporting scientific information, due acknowledgments have been made wherever the findings of others have been cited.

Place: Thiruvananthapuram
Date: January - May 2023

Ajay Daniel Pravin
(SC19B042)

This project report is dedicated to my parents who instilled a sense of explorative curiosity, and all my teachers and lab staff since who armed me with the tools to apply it…

Acknowledgements

Firstly, I would like to thank my advisor and guide, **Dr. Rajesh Sadanandan**, for his constant support and encouragement throughout the project. He provided useful tools and study materials necessary for understanding the subject and completing the project.

I would like to thank the lab staff and other students who offered their time, efforts and guidance necessary for completing the project.

I would also like to thank IIST for bestowing upon me this opportunity to do a project in a field of my interest. This has been a great learning experience and an opportunity to grow personally and academically.

Lastly, I would like to thank my parents who have always been supportive of my endeavours.

Ajay Daniel Pravin

Abstract

This project presents an investigation of the spectral emissions from a swirl-stabilized, non-premixed methane-air flame. The study was conducted to gain a better understanding of the flame characteristics and the spectral emissions of such a flame, which is commonly used in industrial combustion systems. The effects of swirl number and equivalence ratio on the spectral emissions were investigated. The experiments were conducted with three configurations of the swirl burner, each with a different annular gap. The results of this study aim to provide useful information for the reliable development and optimization of combustion systems.

Contents

List of Figures **xiii**

Nomenclature **xv**

1 Introduction **1**

2 Literature Review **2**

2.1 Flame Diagnostic Techniques 2
2.2 Flame Emission Spectroscopy 3
2.3 Chemiluminescence 4
2.4 Swirl Burners 6

3 Experimental Setup **9**

3.1 Spectrometer 9
3.2 Lens 9
3.3 Pre-processing of data 9
3.4 Setup for Bunsen Burner testing 10
3.5 Setup for Swirl Burner 12

4 Diagnostics of variable swirl burner with methane **15**

4.1 Flow conditions 15
4.2 Spectra obtained 17

5 Observations and inferences **26**

5.1 Equivalence Ratio Analysis 26
5.2 ${C_2}^*/CH^*$ Ratio analysis 33
5.3 H_2O Peak analysis 36

6 Results and Conclusion **38**

Bibliography **39**

Appendices **41**

A MATLAB Code **41**

List of Figures

2.1 Swirl flow zones 7

3.1 Background noise for configuration 1 10
3.2 Bunsen burner setup 10
3.3 Radical Peaks - Bunsen Burner 11
3.4 Bunsen Burner Spectra 11
3.6 Swirl burner with Combustor attached 13
3.7 Swirl burner setup 13
3.8 Radical Peaks - Swirl Burner 14

4.3 Spectra obtained for Configuration - 1 19
4.6 Spectra obtained for Configuration - 2 22
4.9 Spectra obtained for Configuration - 3 25

5.4 Radical Peaks vs ϕ for Configuration - 1 28
5.8 Radical Peaks vs ϕ for Configuration - 2 30
5.12 Radical Peaks vs ϕ for Configuration - 3 32
5.13 ${C_2}^*/CH^*$ ratio trend for configuration - 1 33
5.14 ${C_2}^*/CH^*$ ratio trend for configuration - 2 34
5.15 ${C_2}^*/CH^*$ ratio trend for configuration - 3 34
5.16 H_2O peaks trend for configuration - 1 36
5.17 H_2O peaks trend for configuration - 2 36
5.18 H_2O peaks trend for configuration - 3 37

Nomenclature

FES - Flame Emission Spectroscopy
FDT - Flame Diagnostic Techniques
PDT - Plume Diagnostic Techniques
ϕ - Equivalence Ratio
S - Swirl Number

Chapter 1

Introduction

The combustion of fossil fuels is a major contributor to the release of greenhouse gases and air pollution. Thus, there is a pressing need to better understand the fundamental mechanisms of combustion, as well as the associated emissions. Flame spectroscopy is a powerful diagnostic tool for studying the chemical reactions and physical processes occurring in combustion systems. In this technical report, we investigate the spectral emissions from a swirl-stabilized, non-premixed methane/air flame, which is a commonly used combustion configuration.

The swirl-stabilized flame is characterized by a re-circulation zone, which enhances the mixing of fuel and air, leading to a more efficient combustion process. Non-premixed flames, on the other hand, involve separate fuel and oxidizer streams that are mixed and burned in the combustion zone. The combination of swirl stabilization and non-premixed fuel and oxidizer streams leads to a complex combustion process that is not well understood. Therefore, the study of the spectral emissions from this type of flame is of great importance.

We use flame emission spectroscopy (FES) to measure the spectral emissions from the flame. FES allows us to study the chemical species present in the flame, as well as their concentrations and temperature distribution [5,10]. By analyzing the spectral emissions from the flame, we can gain insights into the combustion process and identify the species responsible for the emission of pollutants.

In this study, we vary the equivalence ratio of the flame, which is the ratio of the actual fuel-to-air ratio to the stoichiometric fuel-to-air ratio. This allows us to investigate the effect of variations in the fuel-air mixtures on the spectral emissions from the flame. The results of this study can provide valuable insights into the combustion process of methane/air mixtures, which can be used to optimize combustion systems and reduce pollutant emissions.

Chapter 2

Literature Review

2.1 Flame Diagnostic Techniques

Flame diagnostic techniques (FDT) are tools that allow us to gain a deeper understanding of combustion processes by providing information on various aspects of the flame, such as temperature, species concentration, and flame structure. By analyzing the data obtained from these techniques, researchers can gain insights into the chemical reactions taking place in the flame, as well as the effects of various parameters such as fuel composition, burner design, and operating conditions on the combustion process. This information can then be used to optimize combustion systems for improved efficiency, reduced emissions, and enhanced safety.

There are several types of flame diagnostic techniques such as:

- Spectroscopic Techniques: These measure the spectral radiation emitted by the flame, and can provide information about temperature, species concentration, and other flame characteristics. [1-8]
- Laser Diagnostics: These use laser light to probe the flame, and can provide information about flow velocity, temperature, and species concentration. [7]
- Imaging Techniques: These use high-speed cameras or other imaging devices to capture images of the flame, and can provide information about flame structure, stability, and other characteristics. [9]
- Gas Sampling Techniques: These involve sampling the gas mixture in and around the flame, and can provide information about species concentration and other flame characteristics.

- Probe Techniques: These involve inserting probes into the flame to measure temperature, pressure, and species concentration, and can provide information about flame structure and characteristics. [7]

The paper "Investigation of the characteristics and stability of air-staged flames" by J Ballester et al. [5] presents an experimental study on the characteristics and stability of air-staged flames. The study focuses on the effect of the fuel staging ratio (FSR) and the air staging ratio (ASR) on the flame characteristics and stability.

The experiments were conducted on a premixed swirl-stabilized burner with natural gas as the fuel. The FSR and ASR were varied to investigate their effect on the flame characteristics and stability. The flame structure, flame temperature, and emissions were measured using various diagnostic techniques, including chemiluminescence, laser-induced fluorescence, and gas analysis.

The results showed that increasing the ASR resulted in a decrease in the flame temperature and an increase in the production of nitrogen oxides (NO_x). The increase in NO_x production was due to the increase in the air-fuel ratio in the flame. On the other hand, increasing the FSR resulted in an increase in the flame temperature and a decrease in NO_x production.

2.2 Flame Emission Spectroscopy

Flame emission spectroscopy (FES) is a type of atomic spectroscopy that is used to analyze the properties of a flame, such as its temperature, composition, and the presence of particular elements or compounds.

The basic principle of flame emission spectroscopy is that atoms or ions in a flame can be excited to higher energy levels by the heat of the flame, and then return to lower energy levels by emitting radiation. Each element has a unique emission spectrum, which can be used to identify the presence of that element in the sample. The intensity of the emitted radiation is proportional to the concentration of the element in the sample.

FES can be more costly and complex to set up than some classical diagnostic methods, such as visual inspection or simple chemical tests. However, it offers several advantages over these methods in terms of accuracy, sensitivity, and speed of analysis. They are:

- High sensitivity: FES can detect trace amounts of elements in a sample, with detection limits in the parts-per-million (ppm) or even parts-per-billion (ppb) range.
- Selectivity: FES is a selective technique that can identify and quantify specific elements in a sample, based on the characteristic emission lines of each element.
- Speed: FES is a fast technique that can provide real-time analysis of samples, with analysis times typically ranging from a few seconds to a few minutes.
- Non-destructive: FES is a non-destructive technique that can be used to analyze samples without altering their chemical or physical properties.
- Versatility: FES can be used to analyze a wide range of sample types, including solids, liquids, and gases.

Spectral methods in FES involve using a spectrometer to measure the intensity and wavelength of the light emitted by the flame across a range of wavelengths. The resulting spectrum contains information about the chemical elements present in the flame, as each element emits light at specific wavelengths or spectral lines.

The spectral lines in the flame emission spectrum can be used to identify the elements present in the flame through a process called spectroscopic analysis. Spectroscopic analysis involves comparing the spectral lines in the emission spectrum of the flame to a database of known spectral lines for different elements. By matching the spectral lines in the flame emission spectrum to those in the database, it is possible to identify the elements present in the flame and to determine their relative concentrations.

2.3 Chemiluminescence

Chemiluminescence is a process where light is emitted from a chemical reaction without producing significant amounts of heat. In other words, it is the emission of light from a chemical reaction that occurs without an external source of energy, such as heat or light. The light emission is a result of a chemical reaction producing excited state molecules or atoms that release energy in the form of light as they return to a lower energy state. [7]

The reaction typically involves a molecule, known as the "luminophore," which has an excited state that is higher in energy than its ground state. When the luminophore undergoes

a chemical reaction, it releases energy that causes it to return to its ground state, and this energy is emitted as light.

The energy levels of the excited and ground states of the luminophore molecule are key to the chemiluminescence mechanism. When the molecule is excited by absorbing energy from a chemical reaction, it enters an excited state with higher energy. This excited state is unstable and has a lower energy than the transition state of the reaction, which means that the energy can be released in the form of light as the molecule returns to its ground state.

The wavelength of the emitted light is related to the difference in energy between the excited and ground states of the luminophore molecule. Different luminophores have different energy levels, which means that they emit different colors of light. The intensity of the emitted light is also related to the energy released during the chemical reaction, and can be affected by factors such as the concentration of reactants and temperature.

The emission wavelengths for CH^* and C2* radicals are typically in the UV and visible range. The dominant emission wavelength of OH^* in a flame is around 308 nm. The prominent emission wavelengths for CH^* are around 431 nm (violet-blue), while for C2* they are around 516 nm (green). The CO_2* continuum spectrum is a broad range of wavelengths of this emitted light, which covers a wide range of the electromagnetic spectrum from ultraviolet to infrared. This is because CO_2 molecules can be excited to many different energy levels, resulting in a large number of possible transitions and emissions at different wavelengths. All the formation routes for excited radicals and their characteristic wavelengths are shown in [7].

The article "Chemiluminescence monitoring in premixed flames of natural gas and its blends with hydrogen" by J. Ballester et al. [6] presents an experimental study of the chemiluminescence properties of natural gas (NG) flames and blends of NG with hydrogen (H_2). The authors used a range of techniques, including flame chemiluminescence imaging, laser-induced fluorescence, and emission spectroscopy, to investigate the chemiluminescence characteristics of these flames and the effects of varying the hydrogen content.

The study found that the addition of hydrogen to natural gas flames led to an increase in the chemiluminescence intensity, which can be attributed to the increased production of radicals in the flame. The authors also observed changes in the flame structure and stability with increasing hydrogen content, with higher levels of hydrogen resulting in a more stable

flame and increased flame length.

It also highlights the potential of using chemiluminescence monitoring as a tool for studying the combustion properties of alternative fuels, such as hydrogen, and for developing more efficient and clean combustion technologies. The results of this study could be useful for researchers and engineers working on the development of low-emission combustion systems and the optimization of natural gas/hydrogen blends for energy production.

In the technical paper "Bio-gas combustion: Chemiluminescence fingerprint" [8], FM Quintino investigates the combustion of bio gas as a renewable fuel source. The study focuses on analyzing the chemiluminescence fingerprint of bio-gas combustion to gain insight into the combustion process and emission characteristics.

The experimental setup involved a premixed bio-gas-air flame stabilized in a cylindrical quartz burner. The chemiluminescence emissions were detected using a photo-multiplier tube and spectrometer, and the spectra were analyzed using Fourier transform analysis.

The study found that the chemiluminescence emissions of bio-gas combustion are distinct from those of traditional hydrocarbon fuels, with unique spectral features indicating the presence of CO_2, H_2O, OH^*, and CH^* radicals. The results also suggest that the combustion process of bio-gas is highly dependent on the equivalence ratio, with changes in the flame structure and emissions observed for different fuel-to-air ratios.

Overall, the study demonstrates the potential of chemiluminescence analysis as a powerful tool for understanding the combustion process and optimizing the performance of bio-gas combustion systems.

2.4 Swirl Burners

Swirl burners are a type of combustion system that use the swirling motion of the airflow to enhance the mixing and combustion of fuel and air. In a swirl burner, the fuel and air are introduced into a combustion chamber through separate ports or nozzles, and then the

swirling motion is created by using vanes, tangential ports, or other methods to impart a rotational velocity to the incoming flow.

The swirling motion of the airflow creates a recirculation zone in the center of the combustion chamber, which promotes the mixing of fuel and air and leads to more efficient and stable combustion. The high shear forces in the recirculation zone also promote the formation of small-scale turbulence, which can enhance the mixing of the reactants and increase the flame surface area. [9]

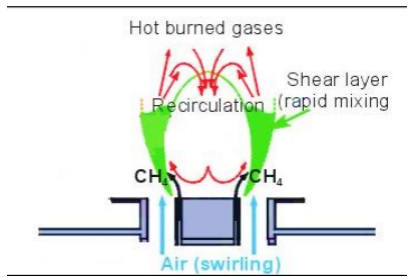

Figure 2.1: Swirl flow zones

Swirl burners are commonly used in a wide range of industrial applications, including furnaces, boilers, gas turbines, and incinerators. They are particularly well-suited for applications that require high combustion efficiency, low emissions, and stable flame operation over a wide range of operating conditions.

Some of the benefits of swirl burners include:

- Improved flame stability: The swirling motion of the airflow promotes better mixing of fuel and air, which leads to more stable combustion and reduced flame instability.
- Reduced emissions: Swirl burners can reduce emissions of pollutants such as nitrogen oxides (NO_x) and carbon moNO_xide (CO) by promoting more complete combustion and reducing flame temperature.
- Increased combustion efficiency: The improved mixing of fuel and air in swirl burners can increase the combustion efficiency and reduce fuel consumption.
- Fuel flexibility: Swirl burners can be designed to accommodate a wide range of fuels, including natural gas, oil, and coal, making them a versatile option for industrial applications.

Variable swirl burners are a type of swirl burner that allow for adjustment of the swirl intensity and direction during operation. This feature makes them highly flexible and versatile, as it enables them to adapt to changing operating conditions and fuel compositions.

Variable swirl burners typically have adjustable vanes or blades that can be rotated to change the swirl intensity and direction. By adjusting these vanes, the flow pattern of the fuel and air can be manipulated to achieve a range of different flame shapes, sizes, and characteristics. This can be particularly useful in applications where flame stability and emissions control are critical, as it allows for fine-tuning of the combustion process to optimize performance and reduce emissions.

One common application of variable swirl burners is in gas turbine engines, where they are used to stabilize the flame and control emissions at different power outputs and altitudes. Another application is in industrial furnaces, where they can be used to improve the efficiency and uniformity of heat transfer by adjusting the flow pattern of the fuel and air. However, swirl burners also have some disadvantages, including higher pressure drop across the combustion chamber, increased complexity of design and manufacturing, and increased maintenance requirements due to the moving parts involved in creating the swirling motion.

Chapter 3

Experimental Setup

3.1 Spectrometer

The spectrometer used is a CCS20 compact USB spectrometer from Thorlabs. It has a spectral range of 200-1100 nm and a spectral resolution of 0.5 nm. The other accessories used from the spectrometer kit include a fiber optic cable, a cuvette holder, and a calibration standard.

3.2 Lens

The lens used is a UV Plano-convex lens with a given focal length of 100 mm (actual focal length is 123 mm). The setup was made such that the fiber optic cable of the spectroscope would lie exactly on the actual focal length. The lens was aligned properly to ensure proper spatial measurements could be taken.

3.3 Pre-processing of data

To ensure accurate data analysis, it is important to pre-process the collected data. This process includes background correction and calibration of the spectrometer. To obtain the background readings, measurements are taken in the same room conditions without the presence of a flame. The corrected values are obtained by subtracting the background readings from the readings obtained for each specific flame condition.

The accuracy of the spectroscope measurement is verified by using a green laser. The laser beam is diffused, and a signal at the 532 nm mark is seen which ensures that the spectroscope can detect signals accurately.

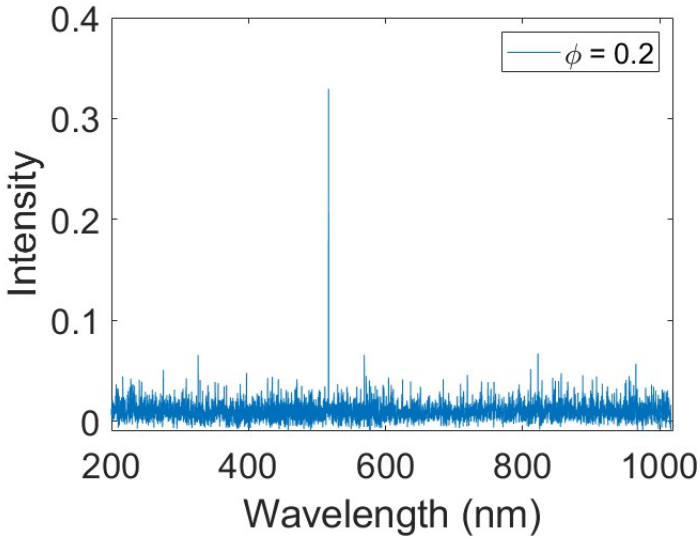

Figure 3.1: Background noise for configuration 1

3.4 Setup for Bunsen Burner testing

To test FES on a Bunsen burner flame, the flame is stabilized and allowed to burn steadily. This flame has a well-defined structure and is therefore an ideal candidate for studying the spectral emissions using FES. LPG was provided as the fuel source and the room was made as dark as possible. The spectra obtained for the tests are displayed for a total of 6 conditions. (0.01 - 0.06 SLPM with 0.01 increment).

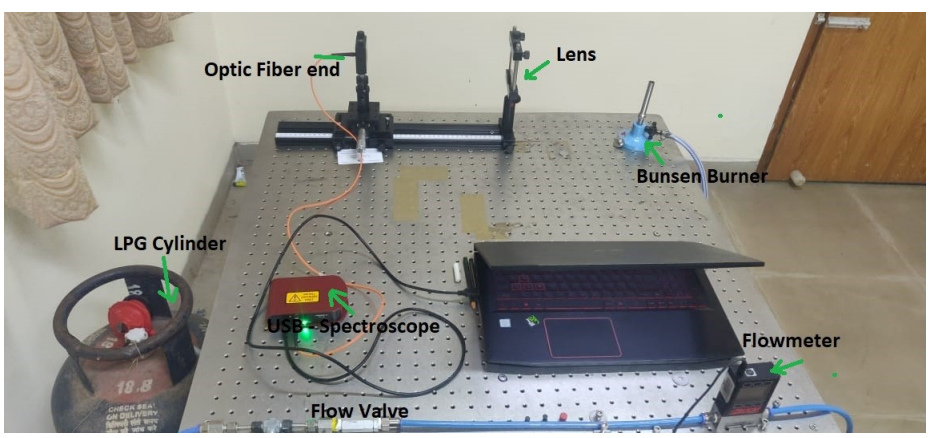

Figure 3.2: Bunsen burner setup

Identification of Radical Peaks

1. 431 nm - this wavelength is associated with emission from CH
2. 516.5 nm - this wavelength is associated with emission from C2

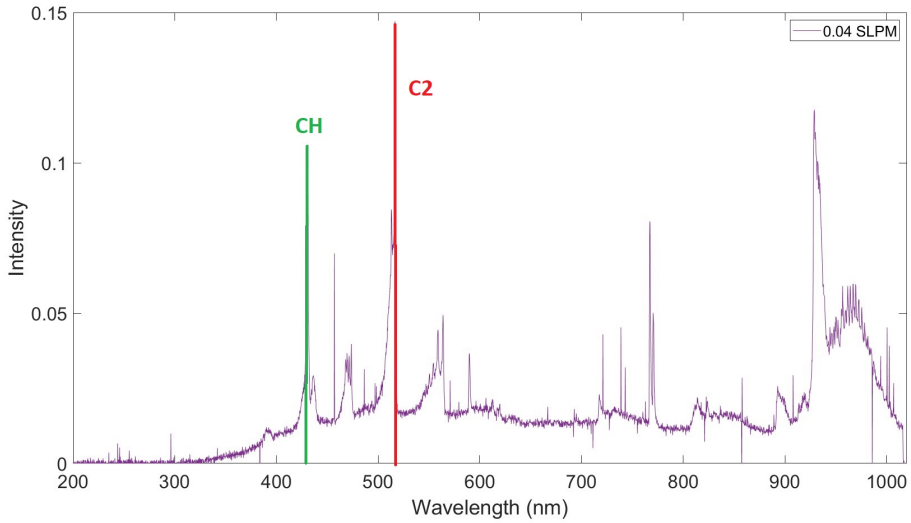

Figure 3.3: Radical Peaks - Bunsen Burner

Spectra

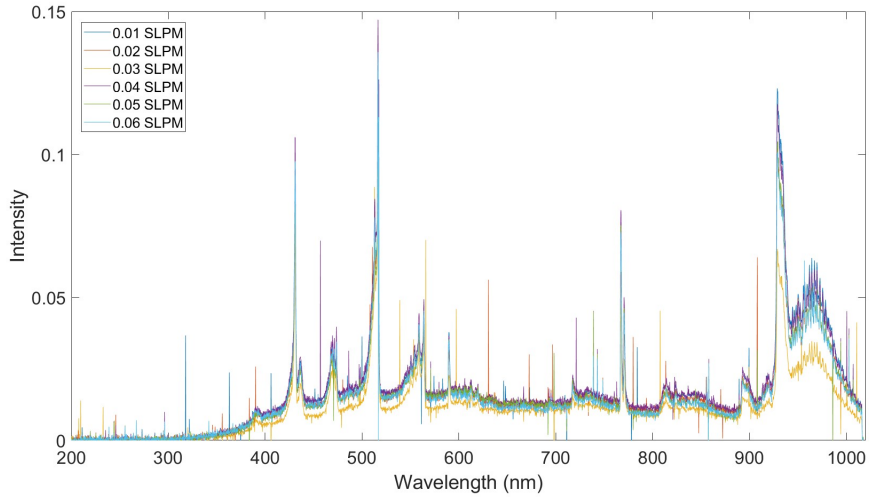

Figure 3.4: Bunsen Burner Spectra

3.5 Setup for Swirl Burner

The burner used is an axial-plus-tangential variable swirl burner IIST-GVS1 with non-premixed configuration. We measure for three configurations of this burner by changing the non-swirling annular gap between the annular nozzle and the central bluff body. These differences are tabulated below:

Burner Configuration	Annular Gap (mm)
IIST-GVS1a	0.5
IIST-GVS1b	0.75
IIST-GVS1c	1.0

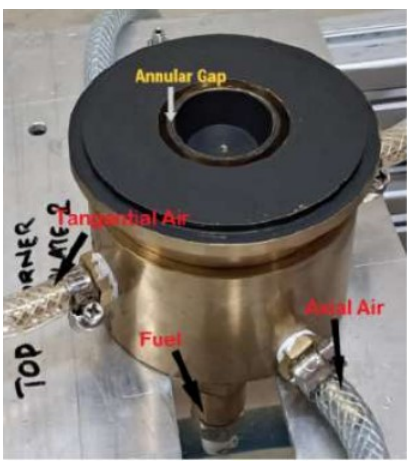

(a) IIST-GVS1 Burner

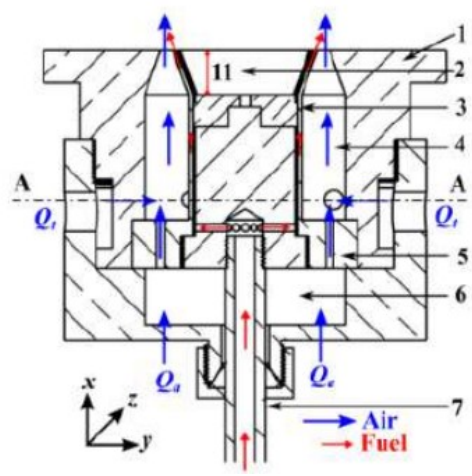

(b) Burner Schematic

There is also a combustor designed in such a way that it fits perfectly with the IIST-GVS1 burner. This metallic cuboid-type structure is designed to simulate flow conditions for practical application. For this experiment, we enable optical access for the spectroscope and camera by using glass panes on two sides.

Figure 3.6: Swirl burner with Combustor attached

The experimental setup is very similar to the Bunsen burner setup but with an additional jack for adjusting the setup height. The fuel used is Methane and the swirl is due to air.

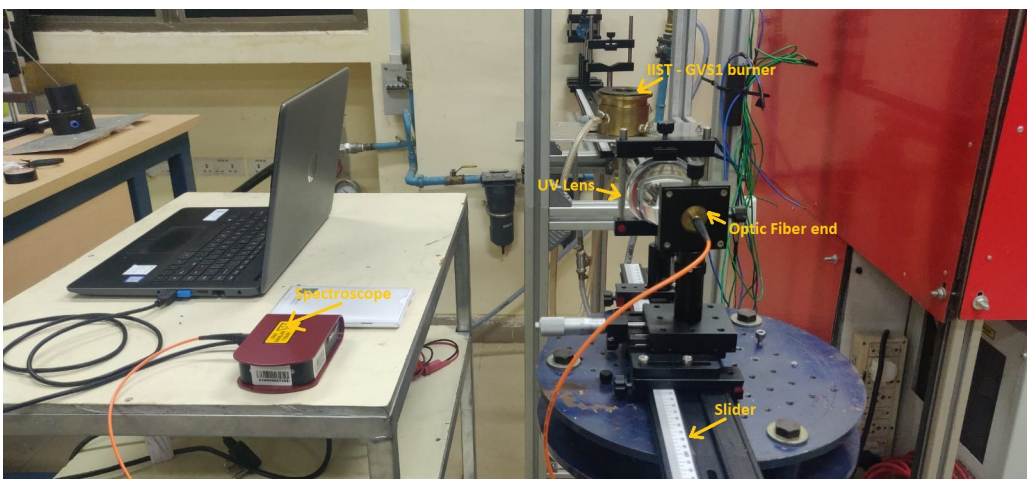

Figure 3.7: Swirl burner setup

We initially identify the spectral lines corresponding to different species using a spectral database. We are able to identify CH, C_2 and H_2O peaks prominently.

Identification of Radical Peaks

1. 431 nm - this wavelength is associated with emission from CH
2. 516.5 nm - this wavelength is associated with emission from C2
3. 892 nm - this wavelength is associated with emission from H_2O (water vapor)

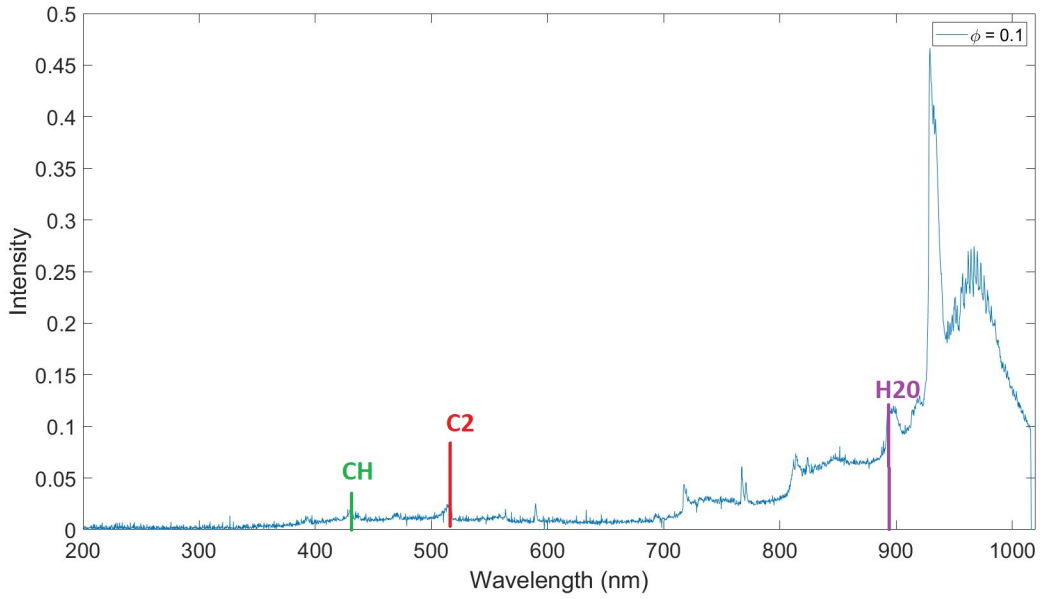

Figure 3.8: Radical Peaks - Swirl Burner

Chapter 4

Diagnostics of variable swirl burner with methane

4.1 Flow conditions

Burner Geometry

We measure for three different configurations of this burner by changing the non-swirling annular gap between the annular nozzle and the central bluff body. These differences are tabulated below:

Burner Configuration	Annular Gap (mm)
IIST-GVS1a	0.5
IIST-GVS1b	0.75
IIST-GVS1c	1.0

Swirl Number

The swirl number (S) is a dimensionless parameter used to quantify the swirling motion in a fluid flow. We use the notation for S as Q_a, Q_t, where Q_a refers to the axial air component and Q_t refers to the tangential air component (each measured in SLPM). We vary S from 100,0 to 0,100 changing each component by 10 SLPM. Therefore we have a total of 11 S conditions for each burner configuration.

Q_a **(SLPM)**	100	90	80	70	60	50	40	30	20	10	0
Q_t **(SLPM)**	0	10	20	30	40	50	60	70	80	90	100

Equivalence Ratio

Equivalence ratio is a parameter commonly used in combustion analysis to describe the fuel-to-air ratio in a flame. It represents the ratio of the actual fuel-to-air ratio to the stoichiometric fuel-to-air ratio required for complete combustion.

The equivalence ratio (ϕ) is varied from 0.1 to 1 at an increment of 0.1. Therefore we have 10 conditions for ϕ for each condition of swirl number.

ϕ	0.1	0.2	0.3	0.4	0.5	0.6	0.7	0.8	0.9	1.0

There are 110 conditions for a single burner configuration, which make 330 cases in total for all configurations. However certain conditions of swirl number and equivalence ratio produce an unstable flame. These conditions will be omitted while capturing the spectra.

4.2 Spectra obtained

4.2.1 Configuration - 1

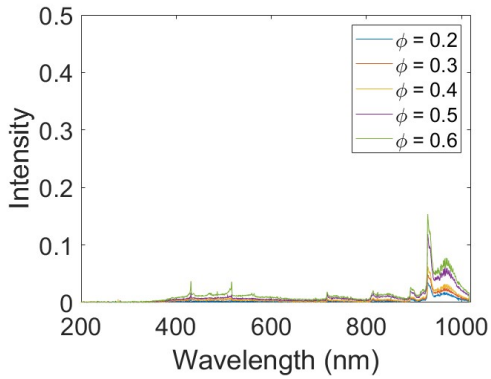

S = 100,0

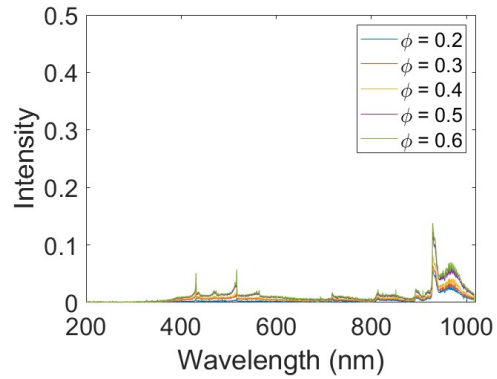

S = 90,10

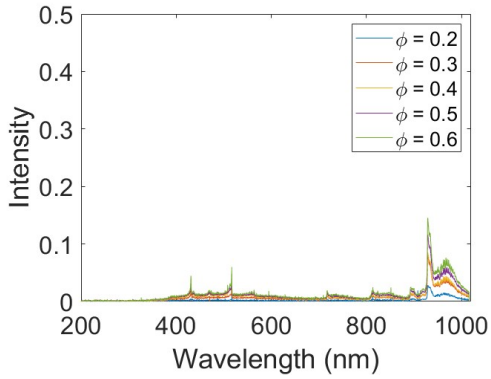

S = 80,20

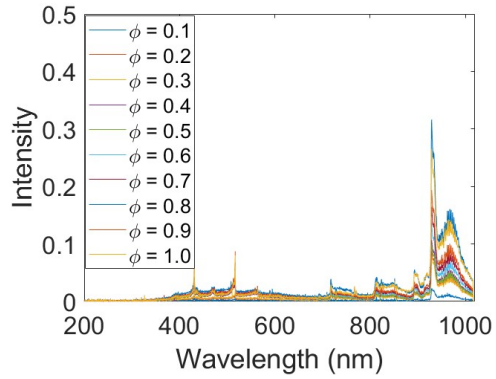

S = 70,30

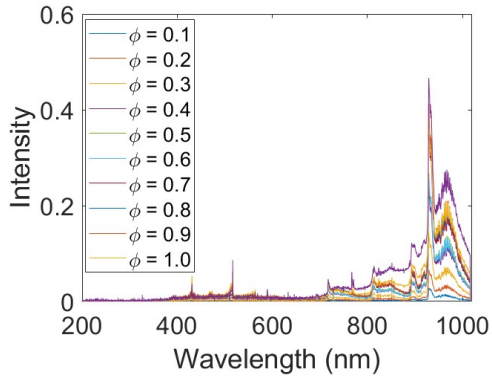

S = 60,40

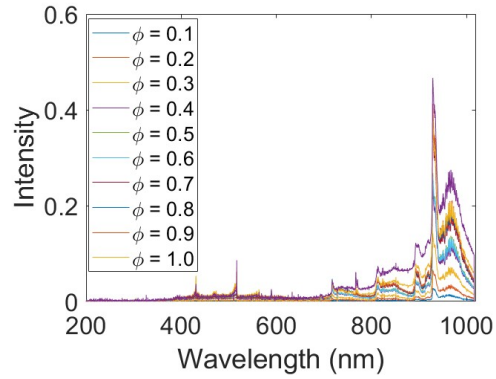

S = 50,50

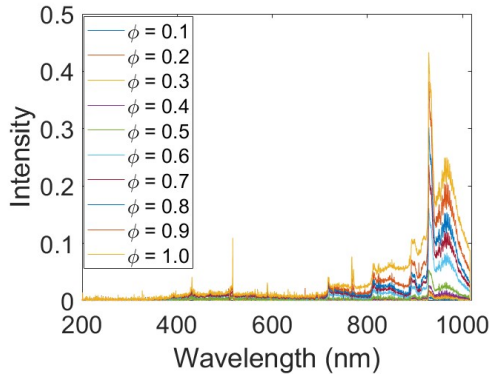

S = 40,60

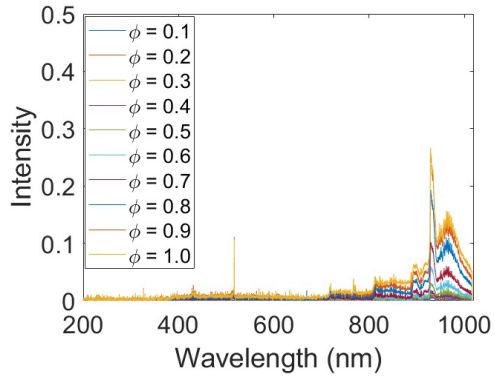

S = 30,70

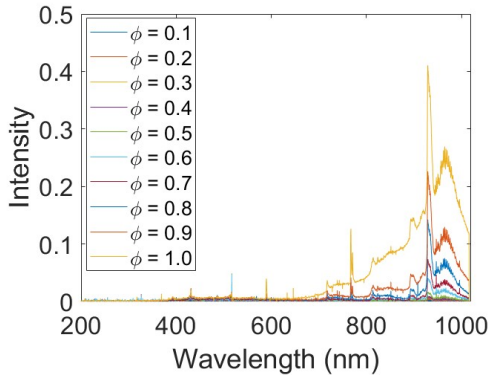

S = 20,80

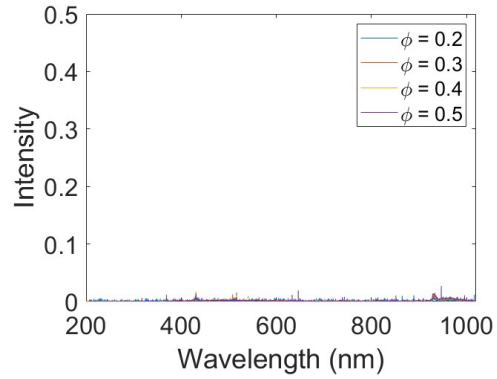

S = 10,90

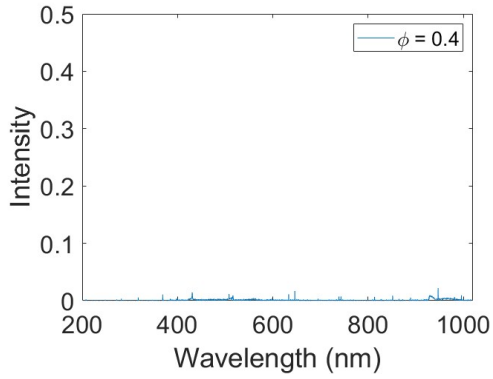

S = 0,100

Figure 4.3: Spectra obtained for Configuration - 1

4.2.2 Configuration - 2

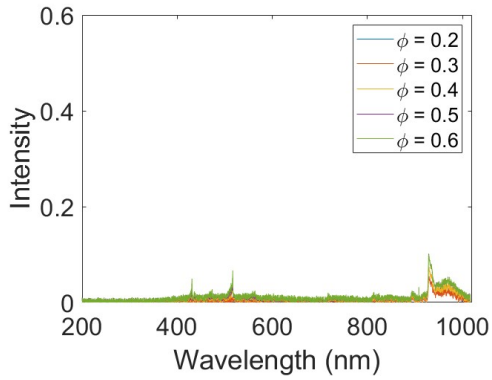

S = 100,0

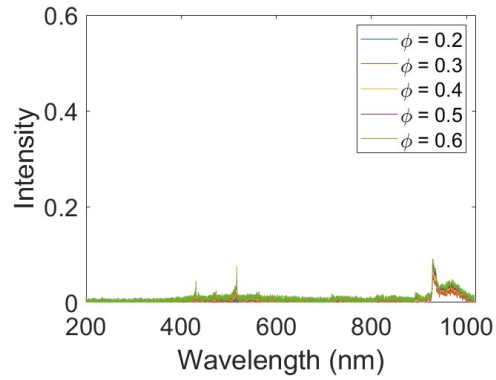

S = 90,10

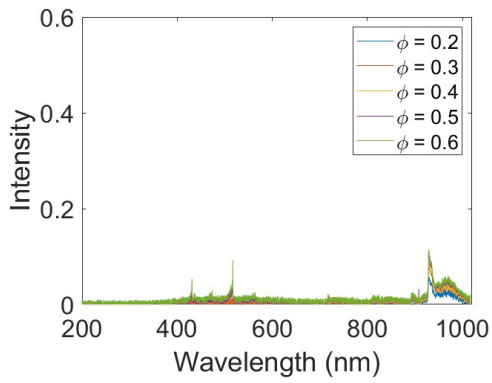

S = 80,20

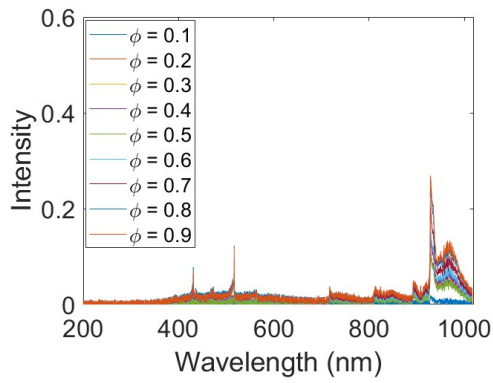

S = 70,30

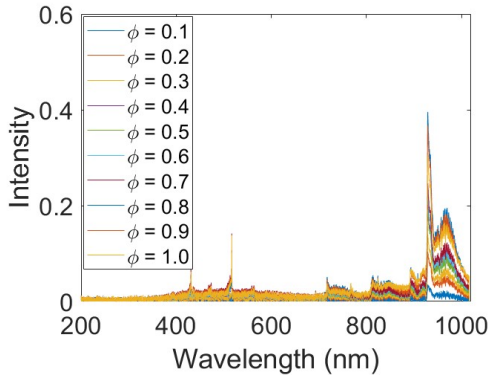

S = 60,40

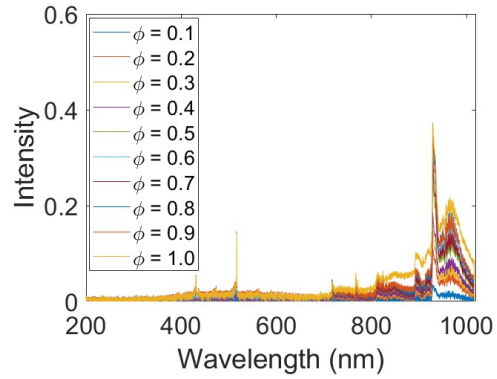

S = 50,50

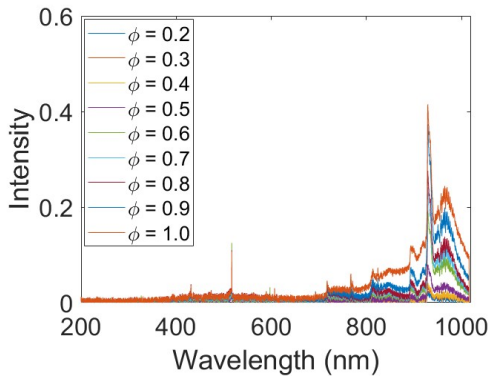

S = 40,60

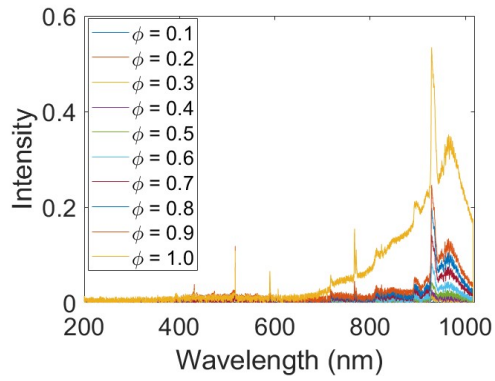

S = 30,70

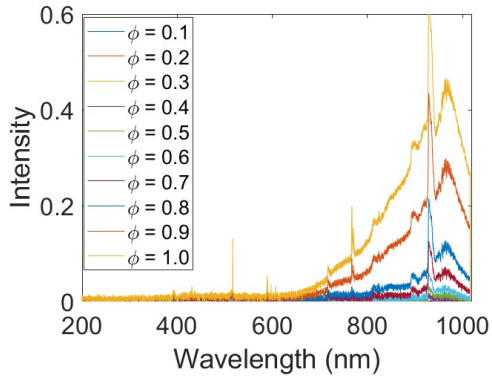

S = 20,80

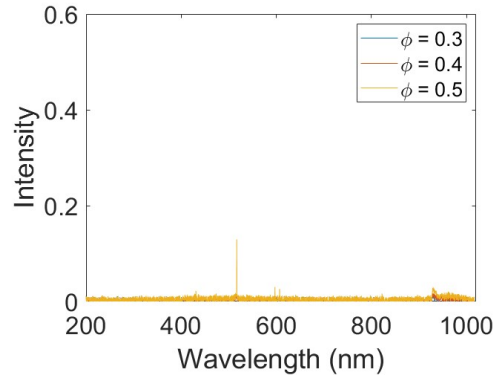

S = 10,90

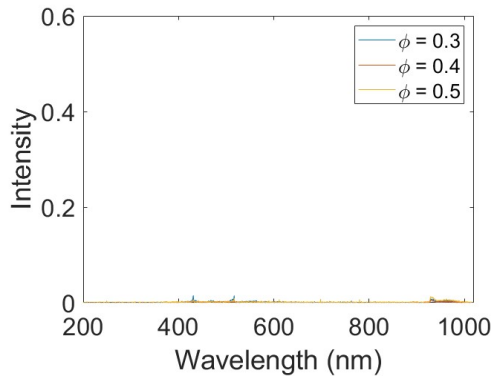

S = 0,100

Figure 4.6: Spectra obtained for Configuration - 2

4.2.3 Configuration - 3

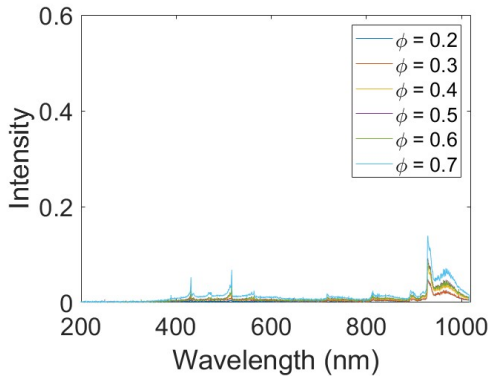

S = 100,0

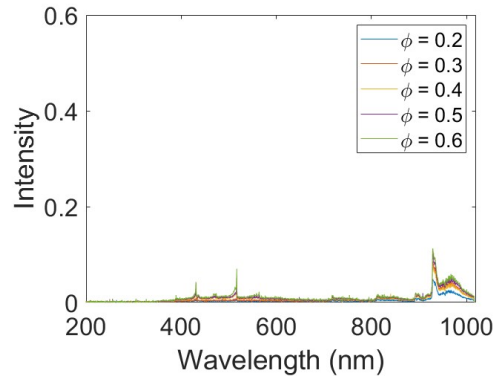

S = 90,10

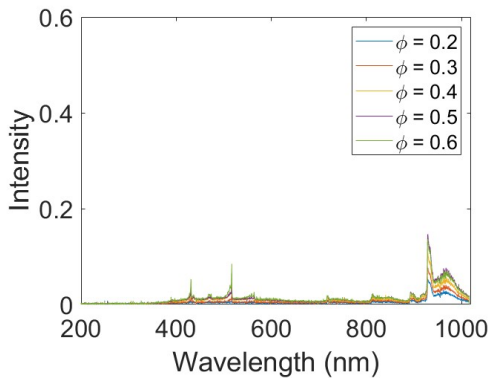

S = 80,20

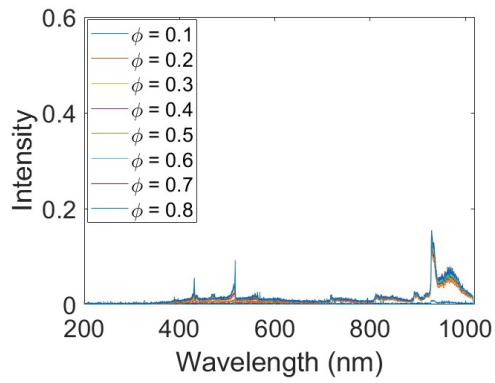

S = 70,30

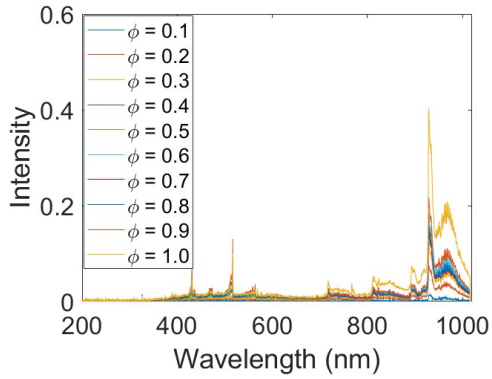

S = 60,40

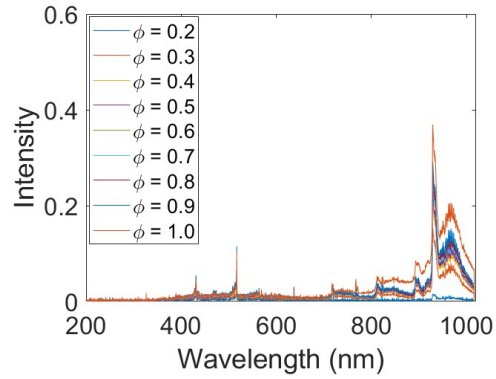

S = 50,50

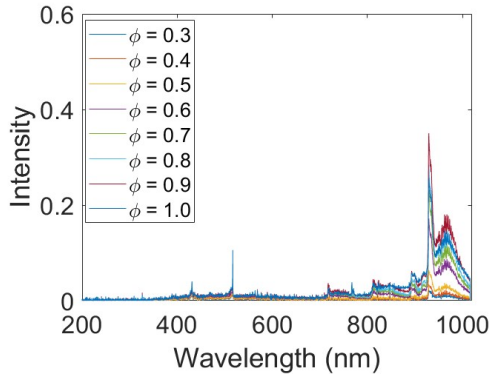

S = 40,60

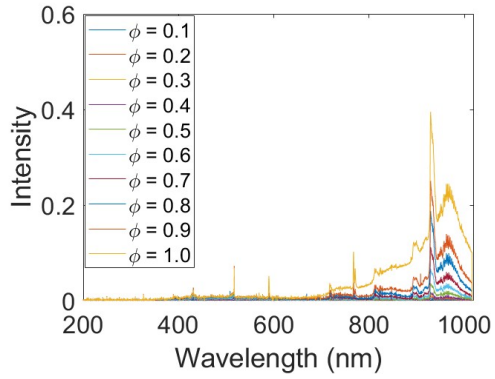

S = 30,70

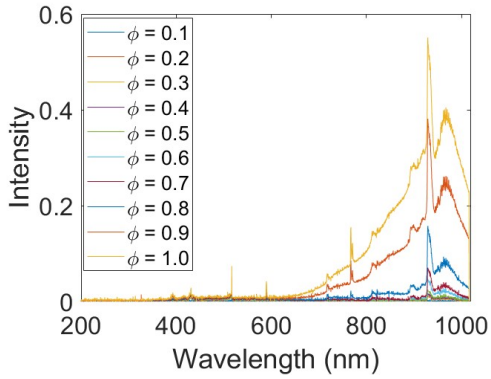

S = 20,80

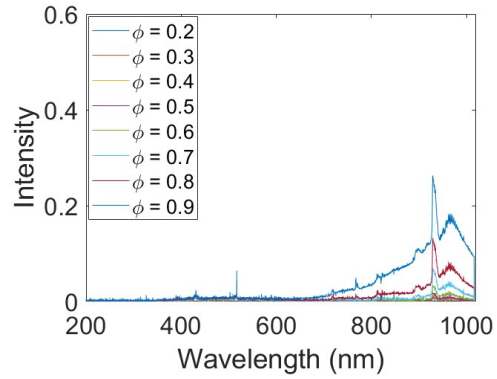

S = 10,90

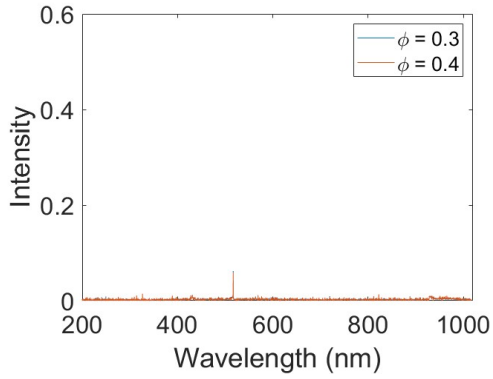

S = 0,100

Figure 4.9: Spectra obtained for Configuration - 3

Chapter 5

Observations and inferences

5.1 Equivalence Ratio Analysis

To analyze the effect of equivalence ratio on the spectral intensities, we fix the swirl number and note the trend in graphs.

5.1.0.1 Configuration - 1

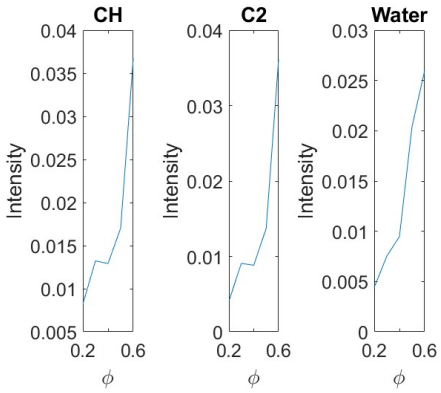

S = 100,0

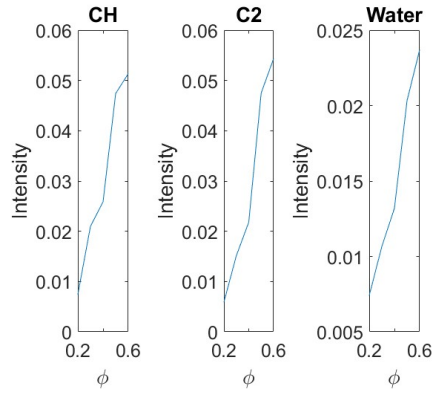

S = 90,10

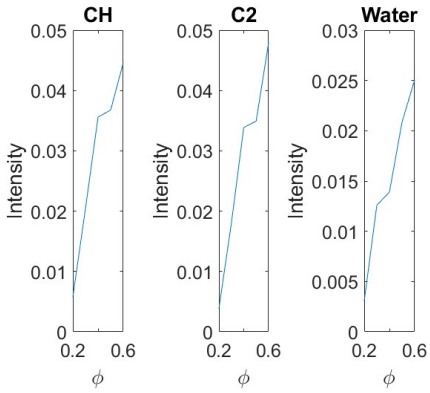

S = 80,20

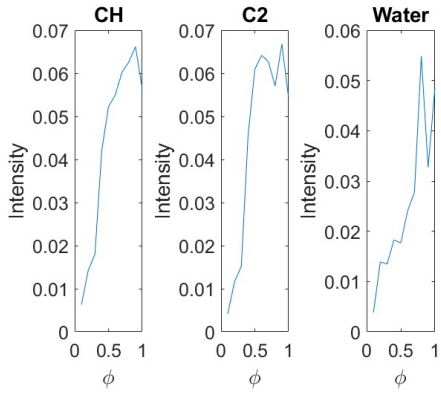

S = 70,30

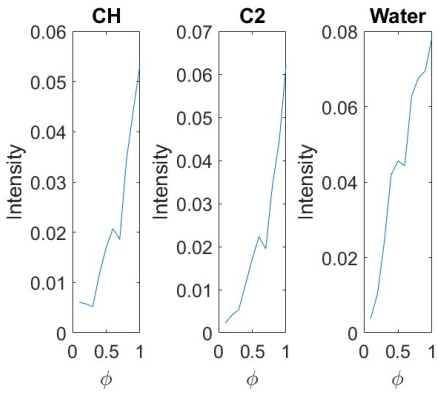

S = 60,40

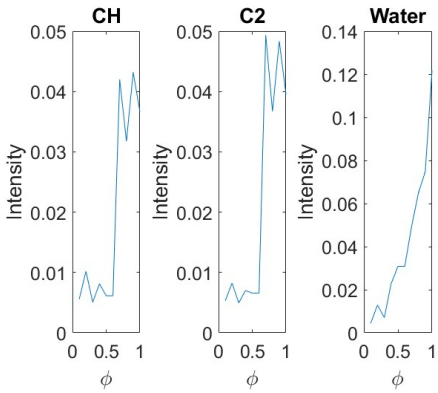

S = 50,50

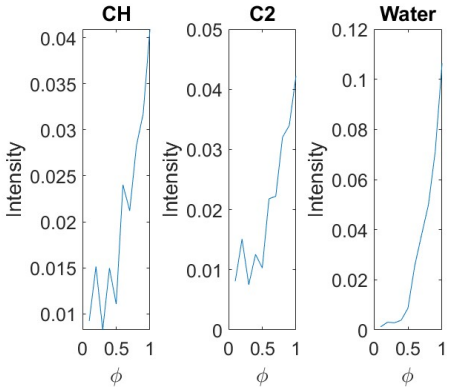

S = 40,60

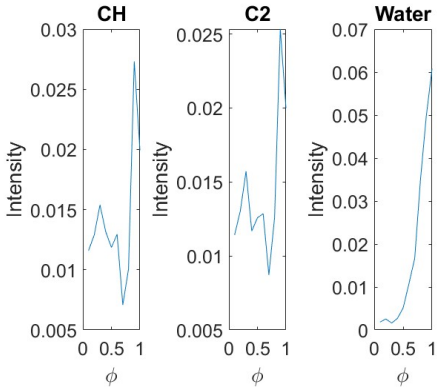

S = 30,70

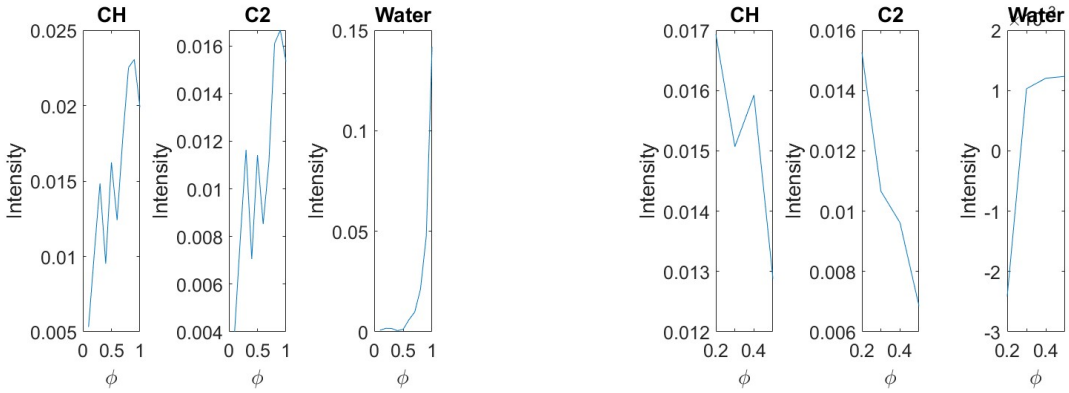

S = 20,80 S = 10,90

Figure 5.4: Radical Peaks vs ϕ for Configuration - 1

5.1.0.2 Configuration - 2

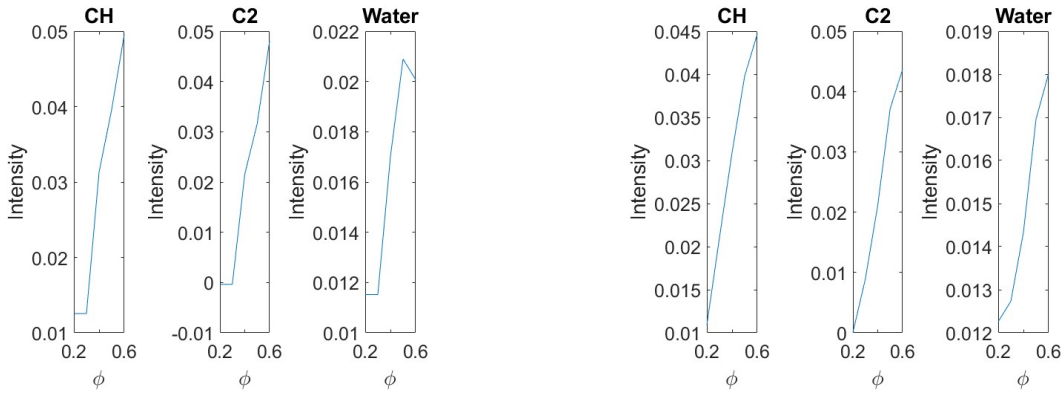

S = 100,0 S = 90,10

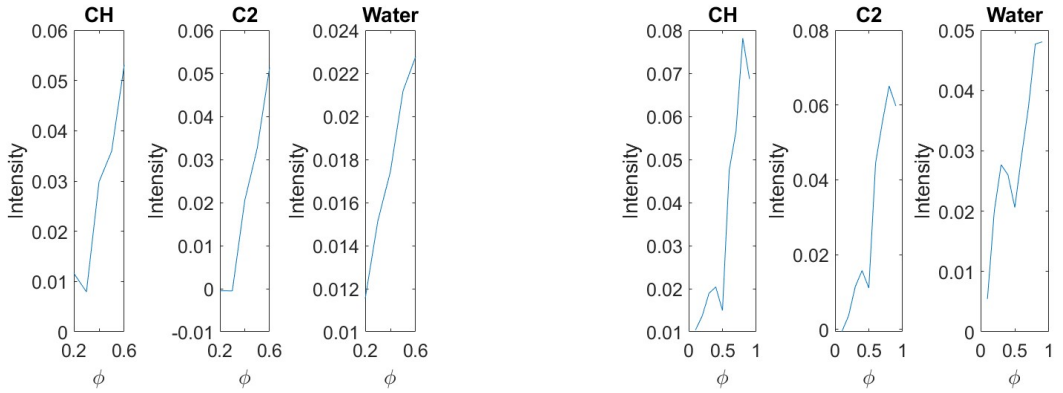

S = 80,20 S = 70,30

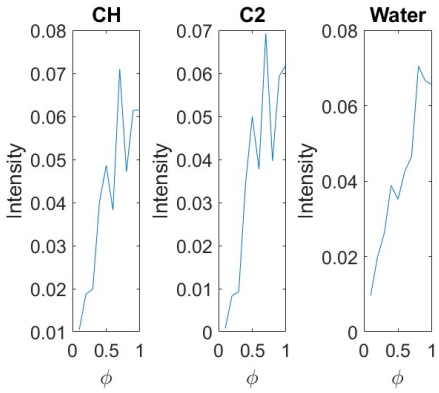

S = 60,40

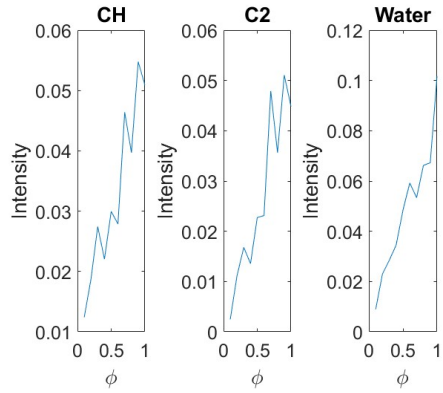

S = 50,50

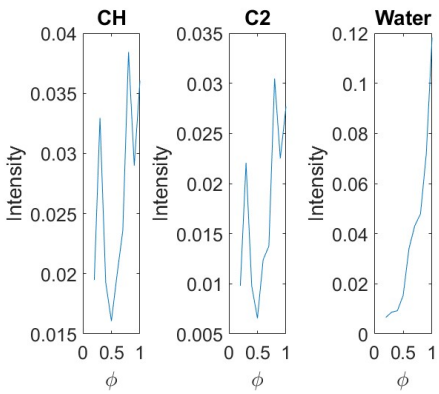

S = 40,60

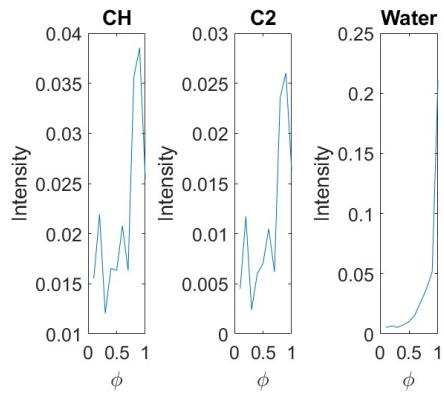

S = 30,70

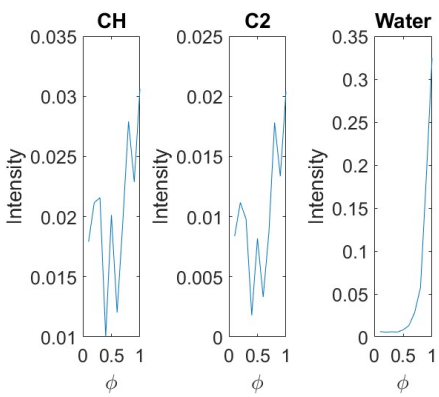

S = 20,80

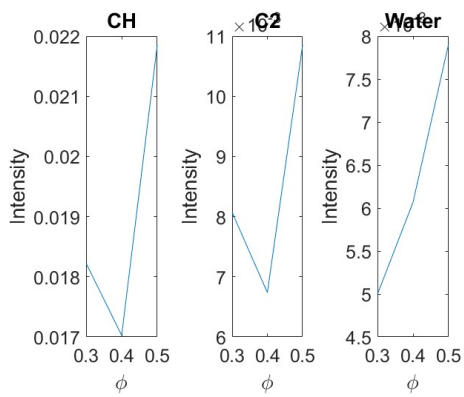

S = 10,90

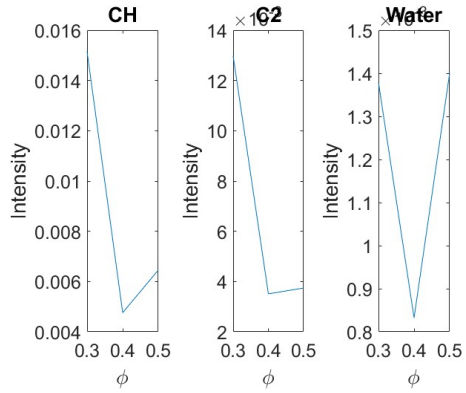

S = 0,100

Figure 5.8: Radical Peaks vs ϕ for Configuration - 2

5.1.0.3 Configuration - 3

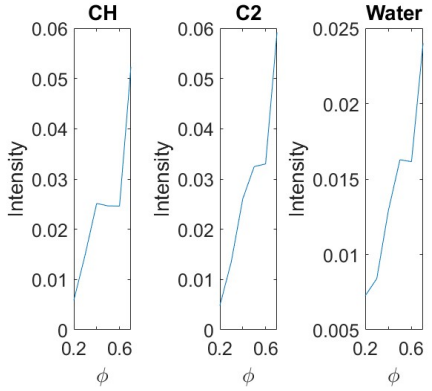

S = 100,0

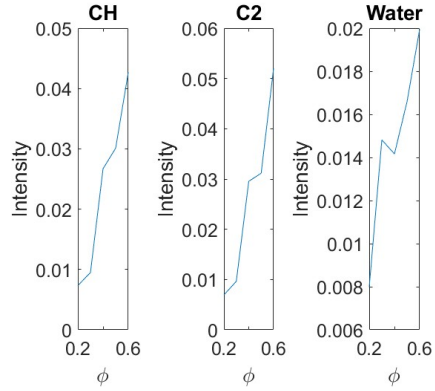

S = 90,10

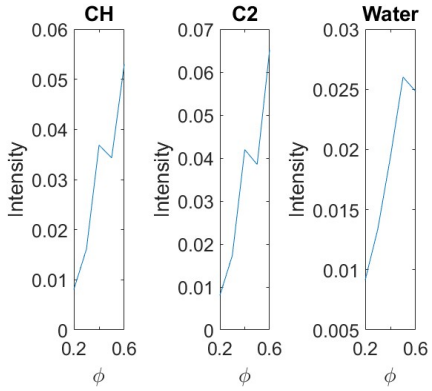

S = 80,20

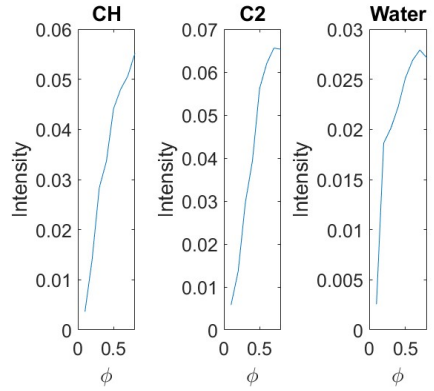

S = 70,30

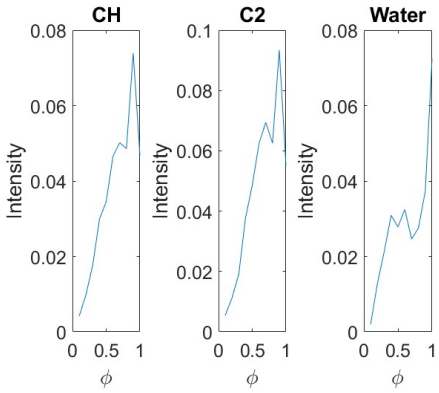

S = 60,40

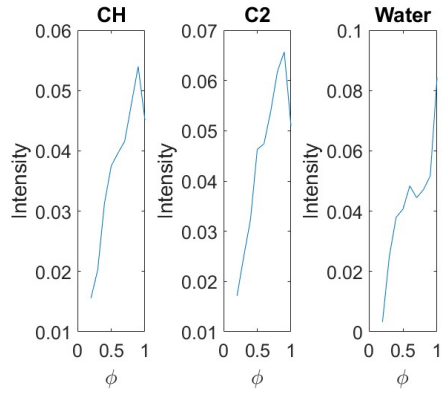

S = 50,50

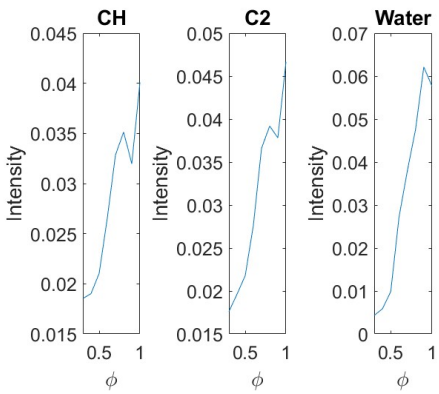

S = 40,60

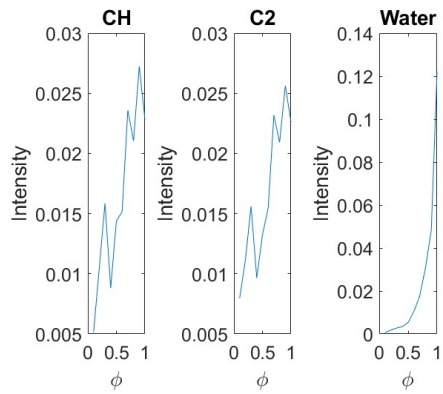

S = 30,70

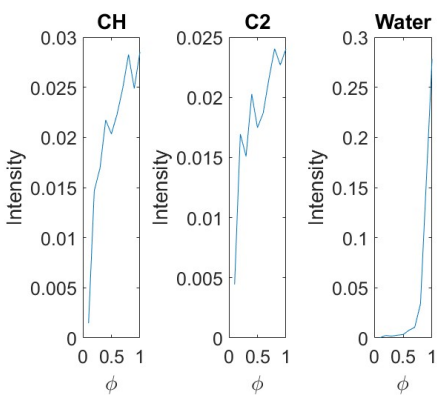

S = 20,80

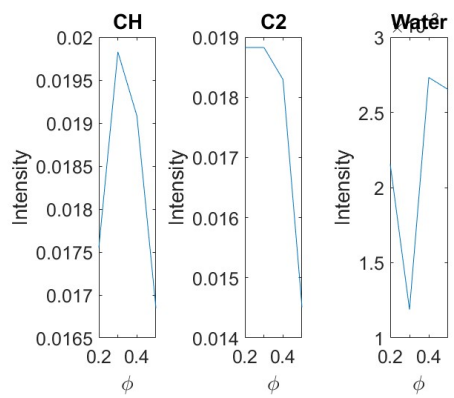

S = 10,90

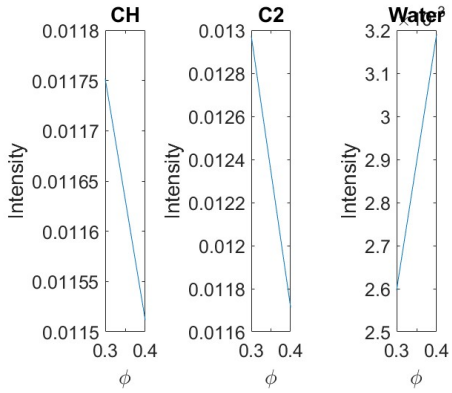

Figure 5.12: Radical Peaks vs ϕ for Configuration - 3

5.1.1 Inferences

Based on the above analysis, we can notice few clear trends and relations between the spectral intensities and equivalence ratio.

1. At S = 100,0 the spectral intensity of the peaks are to an extent proportionally increasing with the equivalence ratio.

2. This proportionality trend still continues till S = 80,20 for water vapor intensities.

3. When the tangential swirl starts increasing, the trend starts to break and finally the trend completely reverses at S = 10,90 for CH and C2 intensities.

4. At S = 0,100, the proportionality trend still holds for water vapor intensities for configurations 1 and 3.

5. At low swirl numbers, the fuel and oxidizer are not well mixed, resulting in incomplete combustion and a low radical peak intensity. As the swirl number increases, the fuel and oxidizer are more efficiently mixed, resulting in better combustion and a higher Radical peak intensity. This trend continues until a certain point, beyond which increasing the swirl number does not improve the mixing further and may even disrupt the combustion process, leading to a decrease in Radical peak intensity.

6. The radical species are produced during the combustion process and their concentration is directly proportional to the amount of fuel being burned. As the equivalence ratio increases, the fuel concentration increases, resulting in a higher Radical peak intensity.

7. When the flow is full tangential (S= 0,100), this can result in incomplete combustion and lower Radical peak intensity explaining the reversing (inverse) proportionality trend.

5.2 $C_2{}^*/CH^*$ Ratio analysis

To obtain more information about the combustion processes in the flame, we plot the $C_2{}^*/CH^*$ ratio against the equivalence ratio for different swirl numbers.

5.2.1 Configuration - 1

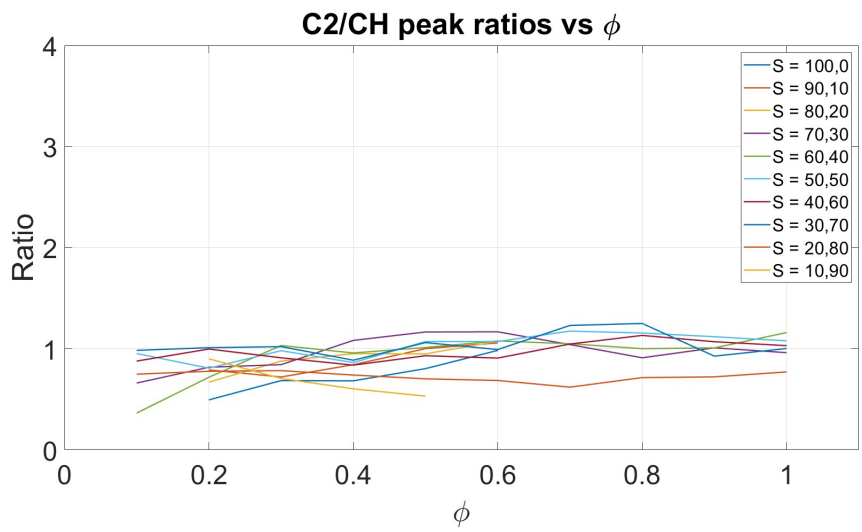

Figure 5.13: $C_2{}^*/CH^*$ ratio trend for configuration - 1

5.2.2 Configuration - 2

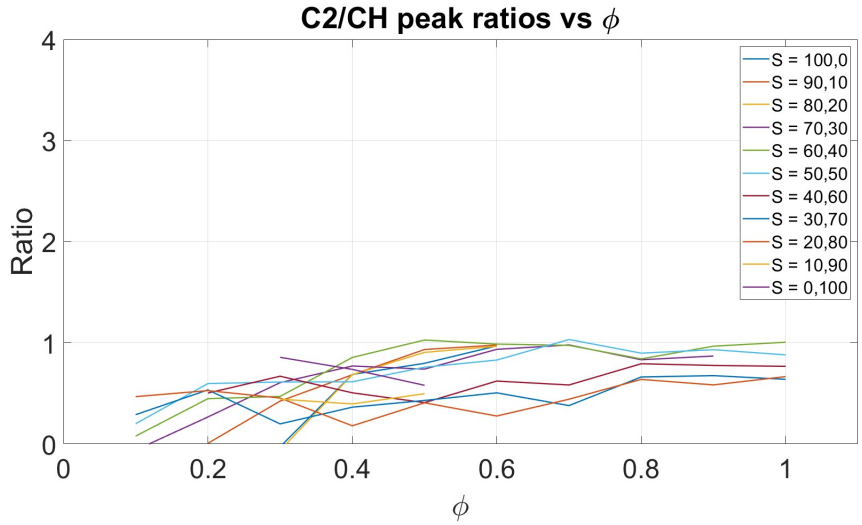

Figure 5.14: ${C_2}^*/CH^*$ ratio trend for configuration - 2

5.2.3 Configuration - 3

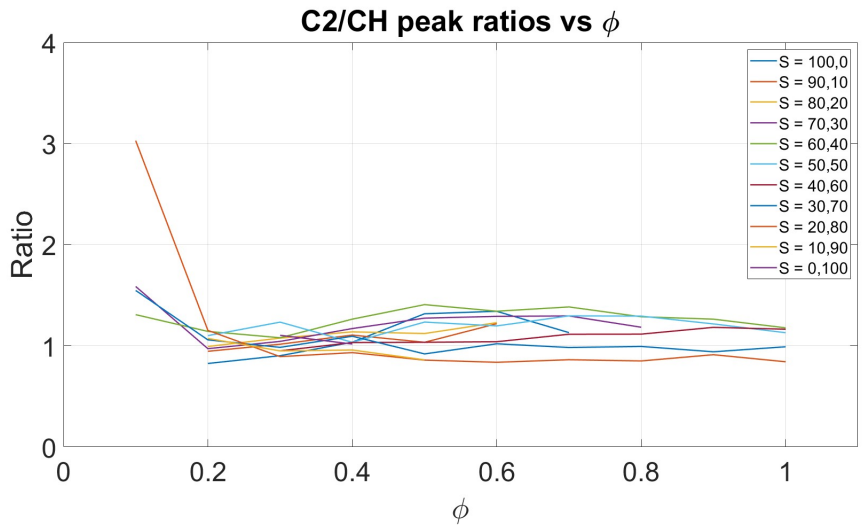

Figure 5.15: ${C_2}^*/CH^*$ ratio trend for configuration - 3

5.2.4 Inferences

1. In configuration 1, only S = 70,30, S = 50,50 and S = 30,70 have points which lie above the value 1 showing C_2 dominance at those points.

2. In configuration-2, almost all of the ${C_2}^*/CH^*$ ratios lie below 1 (higher CH^* intensities) except at one point on S = 60,40.

3. In a fuel-lean environment, there is insufficient methane compared to the available oxygen. As a result, the combustion process may not be complete, and C2* is formed at these conditions.

4. In configuration-3 , the radical ratios are evenly spread above and below 1, with S = 20,80 showing the largest drop in magnitude across ϕ.

5. The consistency of the ${C_2}^*/CH^*$ ratio also can indicate the stability in the flame, with smaller changes in slope showing a more stable flame condition.

6. Configuration 3 has the most steady changes in slopes whereas Configuration 2 is the most sensitive to ϕ.

7. Finally we can get an idea about the concentrations of C_2* and CH^* radicals since they are directly correlated with their peak intensities.

5.3 H_2O Peak analysis

5.3.1 Configuration - 1

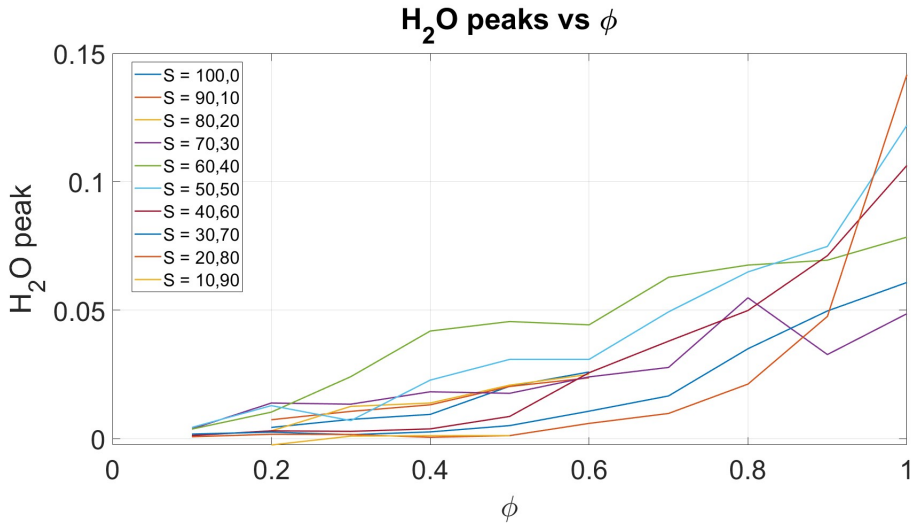

Figure 5.16: H_2O peaks trend for configuration - 1

5.3.2 Configuration - 2

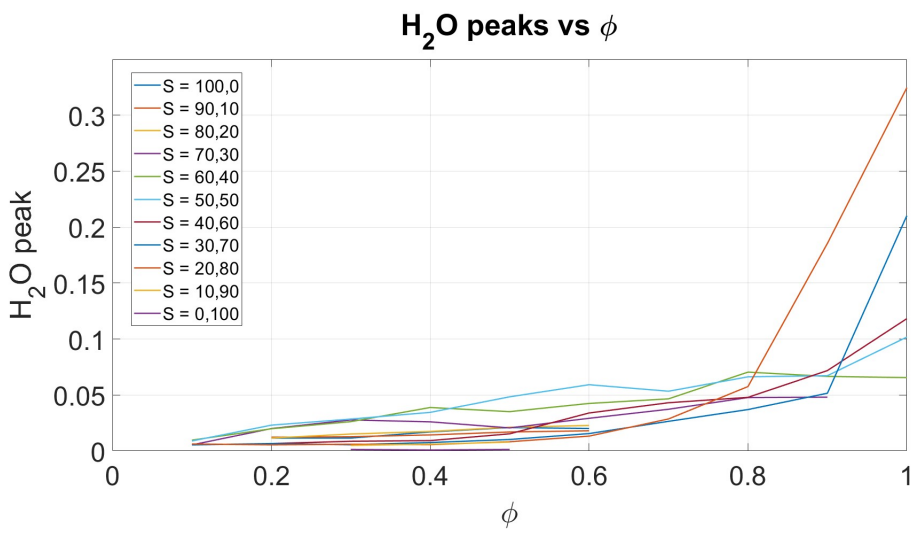

Figure 5.17: H_2O peaks trend for configuration - 2

5.3.3 Configuration - 3

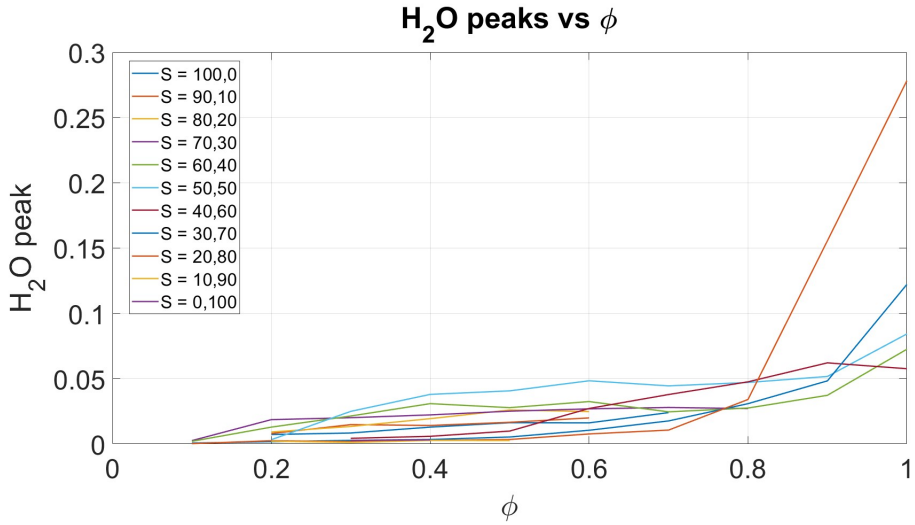

Figure 5.18: H_2O peaks trend for configuration - 3

5.3.4 Inferences

1. The H_2O intensity can serve as an indicator of combustion efficiency. A higher H_2O intensity indicates a greater amount of excited water molecules, which implies a more complete combustion process. Thus, a higher H_2O intensity at higher equivalence ratios suggests improved combustion efficiency.

2. All configurations mostly show an increase in H_2O intensities when the equivalence ratio increases.

Chapter 6

Results and Conclusion

The FES spectra obtained from the non-premixed methane/air flame with swirl-stabilization showed distinct peaks at several wavelengths.

Further analysis of the FES spectra showed a proportionality between the radical peak intensities and the equivalence ratio for swirl numbers with higher axial output. However, as the tangential component increased, this proportionality changed and finally, for a purely tangential swirl, the proportionality became inverse.

This observed trend in the proportionality between radical peak intensities and the equivalence ratio with respect to swirl number highlights the importance of swirl stabilization in controlling the emissions from the flame.

Future Scope of the topic

1. Increasing spatial resolution: While the project used FES to measure spectral emissions from the flame, the spatial resolution could be improved by using higher-resolution spectrometers or by placing the spectrometer closer to the flame. This could provide more detailed information about the flame's structure and dynamics.

2. Investigating pollutant emissions: By analyzing the spectral emissions from the flame, it is possible to estimate the concentration of different chemical species. This could be extended to investigate the emission of pollutants such as nitrogen oxides (NOx) and particulate matter, which have harmful effects on human health and the environment.

3. Modelling the flame: The experimental data obtained from the project could be used

to develop models of the swirl-stabilized, non-premixed flame. These models could be used to predict the flame's behavior under different conditions and optimize burner design for specific applications.

4. Developing control strategies: The data obtained from the project could be used to develop closed-loop control strategies for the flame. By monitoring spectral emissions in real-time and adjusting burner parameters, it may be possible to maintain stable combustion and reduce pollutant emissions.

5. Studying other fuels: The project focused on methane as the fuel for the flame, but other fuels such as propane, butane, and hydrogen could also be studied using the same experimental setup. Comparing the spectral emissions of different fuels could provide valuable insights into the combustion process and help optimize burner design for specific applications.

Bibliography

[1] M Keith Hudson et al *UV, Visible and infrared spectral emissions in Hybrid Rocket Plumes* [1998]

[2] Y. Haralupas, M. Orain *Local measurements of time dependent heat release rate and equivalence ratio using chemiluminescent emission from a flame* [2004]

[3] Arvantes *Design and Implementation of an emission spectroscopy diagnostic in a high-pressure strand burner for the study of solid propellant combustion* [2004]

[4] Edmond W. Wilson et al. *OH Emission Spectra of Hybrid Rocket motors using PMMA and HTPB* [2005]

[5] Javier Ballester et al. *Investigating the characteristics and stability of air-staged flames* [2008]

[6] Javier Ballester et al *Chemiluminescence monitoring in premixed flames of natural gas and its blends with Hydrogen* [2009]

[7] Javier Ballester, Tatiana Garcia Armingol *Diagnostic Techniques for the monitoring and control of practical flames* [2010]

[8] F.M Quintino et al. *Biogas combustion: Chemiluminescence fingerprint* [2018]

[9] Alekseenko et al. *Flow Structure of Swirling Turbulent Propane Flames*

[10] Brieschenk et al. *Chemiluminescence Imaging in Radical-Farming Scramjet* [2013]

[11] Eugene Hecht *Optics* [5th Edition]

Appendix A

MATLAB Code

For obtaining spectra

```
% %Plot - 1
% plot(w, d_ - back);
% legend('\phi = 0.1', '\phi = 0.2','\phi = 0.3', '\phi =
    0.4', '\phi = 0.5','\phi = 0.6', '\phi = 0.7', '\phi =
    0.8', '\phi = 0.9','\phi = 1.0',)

%NOTE:
%431.005 is at position 1123 ---- CH*
%516.416 is at position 1508 ---- C2*
%892.95  is at position 3130 ---- water vapor
%929.1   is at position 3281 ---- hydroxyl
%

load('Var1.mat');
%%
%100
figure(1)
% plot(w, d100_2 - back);
% hold on;
% plot(w, d100_3 - back);
% plot(w, d100_4 - back);
% plot(w, d100_5 - back);
plot(w, d100_6 - back);
```

```
xlim([200,1020]);
% ylim([0,0.7]);
legend('\phi = 0.2','\phi = 0.3', '\phi = 0.4', '\phi = 0.5'
    ,'\phi = 0.6');
%%
%90
figure(2)
plot(w, d90_2 - back);
hold on;
plot(w, d90_3 - back);
plot(w, d90_4 - back);
plot(w, d90_5 - back);
plot(w, d90_6 - back);
xlim([200,1020]);
ylim([0,0.7]);
legend('\phi = 0.2','\phi = 0.3', '\phi = 0.4', '\phi = 0.5'
    ,'\phi = 0.6');
%%
%80
figure(3)
plot(w, d80_2 - back);
hold on;
plot(w, d80_3 - back);
plot(w, d80_4- back);
plot(w, d80_5 - back);
plot(w, d80_6 - back);
xlim([200,1020]);
ylim([0,0.7]);
legend('\phi = 0.2','\phi = 0.3', '\phi = 0.4', '\phi = 0.5'
    ,'\phi = 0.6');
%%
%70
figure(4)
plot(w, d70_1 - back);
hold on
```

```
plot(w, d70_2 - back);
plot(w, d70_3 - back);
plot(w, d70_4 - back);
plot(w, d70_5 - back);
plot(w, d70_6 - back);
plot(w, d70_7 - back);
plot(w, d70_8 - back);
plot(w, d70_9 - back);
plot(w, d70_10 - back);
xlim([200,1020]);
ylim([0,0.7]);
legend('\phi = 0.1','\phi = 0.2','\phi = 0.3', '\phi = 0.4',
    '\phi = 0.5','\phi = 0.6', '\phi = 0.7', '\phi = 0.8', '
   \phi = 0.9', '\phi = 1.0');
%%
%60
figure(5)
plot(w, d60_1 - back);
hold on
plot(w, d60_2 - back);
plot(w, d60_3 - back);
plot(w, d60_4 - back);
plot(w, d60_5 - back);
plot(w, d60_6 - back);
plot(w, d60_7 - back);
plot(w, d60_8 - back);
plot(w, d60_9 - back);
plot(w, d60_10 - back);
xlim([200,1020]);
ylim([0,0.7]);
legend('\phi = 0.1', '\phi = 0.2','\phi = 0.3', '\phi = 0.4'
    , '\phi = 0.5','\phi = 0.6', '\phi = 0.7', '\phi = 0.8',
   '\phi = 0.9','\phi = 1.0');
%%
%50
```

```
figure(6)
plot(w, d60_1 - back);
hold on
plot(w, d50_2 - back);
plot(w, d50_3 - back);
plot(w, d50_4 - back);
plot(w, d50_5 - back);
plot(w, d50_6 - back);
plot(w, d50_7 - back);
plot(w, d50_8 - back);
plot(w, d50_9 - back);
plot(w, d50_10 - back);
xlim([200,1020]);
ylim([0,0.7]);
legend('\phi = 0.1','\phi = 0.2','\phi = 0.3', '\phi = 0.4',
    '\phi = 0.5','\phi = 0.6', '\phi = 0.7', '\phi = 0.8', '
   \phi = 0.9','\phi = 1.0');
%%
%40
figure(7)
plot(w, d40_1 - back);
hold on;
plot(w, d40_2 - back);
plot(w, d40_3 - back);
plot(w, d40_4 - back);
plot(w, d40_5 - back);
plot(w, d40_6 - back);
plot(w, d40_7 - back);
plot(w, d40_8 - back);
plot(w, d40_9 - back);
plot(w, d40_10 - back);
xlim([200,1020]);
ylim([0,0.7]);
legend('\phi = 0.1', '\phi = 0.2', '\phi = 0.3', '\phi = 0.4
   ', '\phi = 0.5','\phi = 0.6', '\phi = 0.7', '\phi = 0.8',
```

```
    '\phi = 0.9','\phi = 1.0');
%%
%30
figure(8)
plot(w, d30_1 - back);
hold on
plot(w, d30_2 - back);
plot(w, d30_3 - back);
plot(w, d30_4 - back);
plot(w, d30_5 - back);
plot(w, d30_6 - back);
plot(w, d30_7 - back);
plot(w, d30_8 - back);
plot(w, d30_9 - back);
plot(w, d30_10 - back);
xlim([200,1020]);
ylim([0,0.7]);
legend('\phi = 0.1', '\phi = 0.2', '\phi = 0.3', '\phi = 0.4
    ', '\phi = 0.5','\phi = 0.6', '\phi = 0.7', '\phi = 0.8',
     '\phi = 0.9','\phi = 1.0');
%%
%%20
figure(9)
plot(w, d20_1 - back);
hold on
plot(w, d20_2 - back);
plot(w, d20_3 - back);
plot(w, d20_4 - back);
plot(w, d20_5 - back);
plot(w, d20_6 - back);
plot(w, d20_7 - back);
plot(w, d20_8 - back);
plot(w, d20_9 - back);
plot(w, d20_10 - back);
xlim([200,1020]);
```

```
ylim([0,0.7]);
legend('\phi = 0.1', '\phi = 0.2', '\phi = 0.3', '\phi = 0.4
    ', '\phi = 0.5','\phi = 0.6', '\phi = 0.7','\phi = 0.8',
    '\phi = 0.9','\phi = 1.0');
%%
%%10
figure(10)
plot(w, d10_2 - back);
hold on
plot(w, d10_3 - back);
plot(w, d10_4 - back);
plot(w, d10_5 - back);
xlim([200,1020]);
ylim([0,0.7]);
legend('\phi = 0.2', '\phi = 0.3', '\phi = 0.4', '\phi = 0.5
    ');
%%
%0
figure(11)
plot(w, d0_4 - back);
xlim([200,1020]);
ylim([0,0.7]);
legend('\phi = 0.4');\\
```

noindent **For obtaining radical peak trends**

```

%NOTE:
%431.005 is at position 1123 ---- CH*
%516.416 is at position 1508 ---- C2*
%892.95  is at position 3130 ---- water vapor
%929.1   is at position 3281 ---- hydroxyl
load('Var1.mat');

%CH
```

```
%%%
```

```
plot(eq100, hy100)
title('Hydroxyl peaks ve equivalence ratio')
xlabel('\phi');

%%
%%90
figure(2)
ch90 = [d90_2(1123)-back(1123),d90_3(1123)-back(1123),d90_4
    (1123)-back(1123),d90_5(1123)-back(1123), d90_6(1123)-
    back(1123)];
cc90 = [d90_2(1508)-back(1508),d90_3(1508)-back(1508),d90_4
    (1508)-back(1508),d90_5(1508)-back(1508), d90_6(1508)-
    back(1508)];
wv90 = [d90_2(3130)-back(3130),d90_3(3130)-back(3130),d90_4
    (3130)-back(3130),d90_5(3130)-back(3130), d90_6(3130)-
    back(3130)];
hy90 = [d90_2(3281)-back(3281),d90_3(3281)-back(3281),d90_4
    (3281)-back(3281),d90_5(3281)-back(3281), d90_6(3281)-
    back(3281)];
eq90 = [0.2, 0.3, 0.4, 0.5, 0.6];
xlabel('\phi');

subplot(2, 2, 1)
plot(eq90, ch90)
title('CH peaks ve equivalence ratio')
xlabel('\phi');

subplot(2, 2, 2)
plot(eq90, cc90)
title('C2 peaks ve equivalence ratio')
xlabel('\phi');

subplot(2, 2, 3)
plot(eq90, wv90)
title('Water vapor peaks ve equivalence ratio')
```

```
xlabel('\phi');

subplot(2, 2, 4)
plot(eq90, hy90)
title('Hydroxyl peaks ve equivalence ratio')
xlabel('\phi');

%%
%%80
figure(3)
ch80 = [d80_2(1123)-back(1123),d80_3(1123)-back(1123),d80_4
    (1123)-back(1123),d80_5(1123)-back(1123), d80_6(1123)-
    back(1123)];
cc80 = [d80_2(1508)-back(1508),d80_3(1508)-back(1508),d80_4
    (1508)-back(1508),d80_5(1508)-back(1508), d80_6(1508)-
    back(1508)];
wv80 = [d80_2(3130)-back(3130),d80_3(3130)-back(3130),d80_4
    (3130)-back(3130),d80_5(3130)-back(3130), d80_6(3130)-
    back(3130)];
hy80 = [d80_2(3281)-back(3281),d80_3(3281)-back(3281),d80_4
    (3281)-back(3281),d80_5(3281)-back(3281), d80_6(3281)-
    back(3281)];
eq80 = [0.2, 0.3, 0.4, 0.5, 0.6];

subplot(2, 2, 1)
plot(eq80, ch80)
title('CH peaks ve equivalence ratio')
xlabel('\phi');

subplot(2, 2, 2)
plot(eq80, cc80)
title('C2 peaks ve equivalence ratio')
xlabel('\phi');

subplot(2, 2, 3)
```

```
plot(eq80, wv80)
title('Water vapor peaks ve equivalence ratio')
xlabel('\phi');

subplot(2, 2, 4)
plot(eq80, hy80)
title('Hydroxyl peaks ve equivalence ratio')
xlabel('\phi');

%%
%%70
figure(4)
ch70 = [d70_1(1123)-back(1123),d70_2(1123)-back(1123),d70_3
    (1123)-back(1123),d70_4(1123)-back(1123),d70_5(1123)-back
    (1123), d70_6(1123)-back(1123),d70_7(1123)-back(1123),
    d70_8(1123)-back(1123),d70_9(1123)-back(1123),d70_10
    (1123)-back(1123)];
cc70 = [d70_1(1508)-back(1508),d70_2(1508)-back(1508),d70_3
    (1508)-back(1508),d70_4(1508)-back(1508),d70_5(1508)-back
    (1508), d70_6(1508)-back(1508),d70_7(1508)-back(1508),
    d70_8(1508)-back(1508),d70_9(1508)-back(1508),d70_10
    (1508)-back(1508)];
wv70 = [d70_1(3130)-back(3130),d70_2(3130)-back(3130),d70_3
    (3130)-back(3130),d70_4(3130)-back(3130),d70_5(3130)-back
    (3130), d70_6(3130)-back(3130),d70_7(3130)-back(3130),
    d70_8(3130)-back(3130),d70_9(3130)-back(3130),d70_10
    (3130)-back(3130)];
hy70 = [d70_1(3281)-back(3281),d70_2(3281)-back(3281),d70_3
    (3281)-back(3281),d70_4(3281)-back(3281),d70_5(3281)-back
    (3281), d70_6(3281)-back(3281),d70_7(3281)-back(3281),
    d70_8(3281)-back(3281),d70_9(3281)-back(3281),d70_10
    (3281)-back(3281)];
eq70 = [0.1, 0.2, 0.3, 0.4, 0.5, 0.6, 0.7, 0.8, 0.9, 1.0];

subplot(2, 2, 1)
```

```
plot(eq70, ch70)
title('CH peaks ve equivalence ratio')
xlabel('\phi');

subplot(2, 2, 2)
plot(eq70, cc70)
title('C2 peaks ve equivalence ratio')
xlabel('\phi');

subplot(2, 2, 3)
plot(eq70, wv70)
title('Water vapor peaks ve equivalence ratio')
xlabel('\phi');

subplot(2, 2, 4)
plot(eq70, hy70)
title('Hydroxyl peaks ve equivalence ratio')
xlabel('\phi');

%%
%%60
figure(5)
ch60 = [d60_1(1123)-back(1123),d60_2(1123)-back(1123),d60_3
    (1123)-back(1123),d60_4(1123)-back(1123),d60_5(1123)-back
    (1123), d60_6(1123)-back(1123),d60_7(1123)-back(1123),
    d60_8(1123)-back(1123),d60_9(1123)-back(1123),d60_10
    (1123)-back(1123)];
cc60 = [d60_1(1508)-back(1508),d60_2(1508)-back(1508),d60_3
    (1508)-back(1508),d60_4(1508)-back(1508),d60_5(1508)-back
    (1508), d60_6(1508)-back(1508),d60_7(1508)-back(1508),
    d60_8(1508)-back(1508),d60_9(1508)-back(1508),d60_10
    (1508)-back(1508)];
wv60 = [d60_1(3130)-back(3130),d60_2(3130)-back(3130),d60_3
    (3130)-back(3130),d60_4(3130)-back(3130),d60_5(3130)-back
    (3130), d60_6(3130)-back(3130),d60_7(3130)-back(3130),
```

```
d60_8(3130)-back(3130),d60_9(3130)-back(3130),d60_10
(3130)-back(3130)];
hy60 = [d60_1(3281)-back(3281),d60_2(3281)-back(3281),d60_3
(3281)-back(3281),d60_4(3281)-back(3281),d60_5(3281)-back
(3281), d60_6(3281)-back(3281),d60_7(3281)-back(3281),
d60_8(3281)-back(3281),d60_9(3281)-back(3281),d60_10
(3281)-back(3281)];
eq60 = [0.1, 0.2, 0.3, 0.4, 0.5, 0.6, 0.7, 0.8, 0.9, 1.0];

subplot(2, 2, 1)
plot(eq60, ch60)
title('CH peaks ve equivalence ratio')
xlabel('\phi');

subplot(2, 2, 2)
plot(eq60, cc60)
title('C2 peaks ve equivalence ratio')
xlabel('\phi');

subplot(2, 2, 3)
plot(eq60, wv60)
title('Water vapor peaks ve equivalence ratio')
xlabel('\phi');

subplot(2, 2, 4)
plot(eq60, hy60)
title('Hydroxyl peaks ve equivalence ratio')
xlabel('\phi');

%%
%%50
figure(6)
ch50 = [d50_1(1123)-back(1123),d50_2(1123)-back(1123),d50_3
(1123)-back(1123),d50_4(1123)-back(1123),d50_5(1123)-back
(1123), d50_6(1123)-back(1123),d50_7(1123)-back(1123),
```

```
d50_8(1123)-back(1123),d50_9(1123)-back(1123),d50_10
(1123)-back(1123)];
cc50 = [d50_1(1508)-back(1508),d50_2(1508)-back(1508),d50_3
(1508)-back(1508),d50_4(1508)-back(1508),d50_5(1508)-back
(1508), d50_6(1508)-back(1508),d50_7(1508)-back(1508),
d50_8(1508)-back(1508),d50_9(1508)-back(1508),d50_10
(1508)-back(1508)];
wv50 = [d50_1(3130)-back(3130),d50_2(3130)-back(3130),d50_3
(3130)-back(3130),d50_4(3130)-back(3130),d50_5(3130)-back
(3130), d50_6(3130)-back(3130),d50_7(3130)-back(3130),
d50_8(3130)-back(3130),d50_9(3130)-back(3130),d50_10
(3130)-back(3130)];
hy50 = [d50_1(3281)-back(3281),d50_2(3281)-back(3281),d50_3
(3281)-back(3281),d50_4(3281)-back(3281),d50_5(3281)-back
(3281), d50_6(3281)-back(3281),d50_7(3281)-back(3281),
d50_8(3281)-back(3281),d50_9(3281)-back(3281),d50_10
(3281)-back(3281)];
eq50 = [0.1, 0.2, 0.3, 0.4, 0.5, 0.6, 0.7, 0.8, 0.9, 1.0];

subplot(2, 2, 1)
plot(eq50, ch50)
title('CH peaks ve equivalence ratio')
xlabel('\phi');

subplot(2, 2, 2)
plot(eq50, cc50)
title('C2 peaks ve equivalence ratio')
xlabel('\phi');

subplot(2, 2, 3)
plot(eq50, wv50)
title('Water vapor peaks ve equivalence ratio')
xlabel('\phi');

subplot(2, 2, 4)
```

```
plot(eq50, hy50)
title('Hydroxyl peaks ve equivalence ratio')
xlabel('\phi');

%%
%%40
figure(7)
ch40 = [d40_1(1123)-back(1123),d40_2(1123)-back(1123),d40_3
    (1123)-back(1123),d40_4(1123)-back(1123),d40_5(1123)-back
    (1123), d40_6(1123)-back(1123),d40_7(1123)-back(1123),
    d40_8(1123)-back(1123),d40_9(1123)-back(1123),d40_10
    (1123)-back(1123)];
cc40 = [d40_1(1508)-back(1508),d40_2(1508)-back(1508),d40_3
    (1508)-back(1508),d40_4(1508)-back(1508),d40_5(1508)-back
    (1508), d40_6(1508)-back(1508),d40_7(1508)-back(1508),
    d40_8(1508)-back(1508),d40_9(1508)-back(1508),d40_10
    (1508)-back(1508)];
wv40 = [d40_1(3130)-back(3130),d40_2(3130)-back(3130),d40_3
    (3130)-back(3130),d40_4(3130)-back(3130),d40_5(3130)-back
    (3130), d40_6(3130)-back(3130),d40_7(3130)-back(3130),
    d40_8(3130)-back(3130),d40_9(3130)-back(3130),d40_10
    (3130)-back(3130)];
hy40 = [d40_1(3281)-back(3281),d40_2(3281)-back(3281),d40_3
    (3281)-back(3281),d40_4(3281)-back(3281),d40_5(3281)-back
    (3281), d40_6(3281)-back(3281),d40_7(3281)-back(3281),
    d40_8(3281)-back(3281),d40_9(3281)-back(3281),d40_10
    (3281)-back(3281)];
eq40 = [0.1, 0.2, 0.3, 0.4, 0.5, 0.6, 0.7, 0.8, 0.9, 1.0];

subplot(2, 2, 1)
plot(eq40, ch40)
title('CH peaks ve equivalence ratio')
xlabel('\phi');

subplot(2, 2, 2)
```

```
plot(eq40, cc40)
title('C2 peaks ve equivalence ratio')
xlabel('\phi');

subplot(2, 2, 3)
plot(eq40, wv40)
title('Water vapor peaks ve equivalence ratio')
xlabel('\phi');

subplot(2, 2, 4)
plot(eq40, hy40)
title('Hydroxyl peaks ve equivalence ratio')
xlabel('\phi');

%%
%%30
figure(8)
ch30 = [d30_1(1123)-back(1123),d30_2(1123)-back(1123),d30_3
    (1123)-back(1123),d30_4(1123)-back(1123),d30_5(1123)-back
    (1123), d30_6(1123)-back(1123),d30_7(1123)-back(1123),
    d30_8(1123)-back(1123),d30_9(1123)-back(1123),d30_10
    (1123)-back(1123)];
cc30 = [d30_1(1508)-back(1508),d30_2(1508)-back(1508),d30_3
    (1508)-back(1508),d30_4(1508)-back(1508),d30_5(1508)-back
    (1508), d30_6(1508)-back(1508),d30_7(1508)-back(1508),
    d30_8(1508)-back(1508),d30_9(1508)-back(1508),d30_10
    (1508)-back(1508)];
wv30 = [d30_1(3130)-back(3130),d30_2(3130)-back(3130),d30_3
    (3130)-back(3130),d30_4(3130)-back(3130),d30_5(3130)-back
    (3130), d30_6(3130)-back(3130),d30_7(3130)-back(3130),
    d30_8(3130)-back(3130),d30_9(3130)-back(3130),d30_10
    (3130)-back(3130)];
hy30 = [d30_1(3281)-back(3281),d30_2(3281)-back(3281),d30_3
    (3281)-back(3281),d30_4(3281)-back(3281),d30_5(3281)-back
    (3281), d30_6(3281)-back(3281),d30_7(3281)-back(3281),
```

```
    d30_8(3281)-back(3281),d30_9(3281)-back(3281),d30_10
    (3281)-back(3281)];
eq30 = [0.1, 0.2, 0.3, 0.4, 0.5, 0.6, 0.7, 0.8, 0.9, 1.0];

subplot(2, 2, 1)
plot(eq30, ch30)
title('CH peaks ve equivalence ratio')
xlabel('\phi');

subplot(2, 2, 2)
plot(eq30, cc30)
title('C2 peaks ve equivalence ratio')
xlabel('\phi');

subplot(2, 2, 3)
plot(eq30, wv30)
title('Water vapor peaks ve equivalence ratio')
xlabel('\phi');

subplot(2, 2, 4)
plot(eq30, hy30)
title('Hydroxyl peaks ve equivalence ratio')
xlabel('\phi');

%%
%%20
figure(9)
ch20 = [d20_1(1123)-back(1123),d20_2(1123)-back(1123),d20_3
    (1123)-back(1123),d20_4(1123)-back(1123),d20_5(1123)-back
    (1123), d20_6(1123)-back(1123),d20_7(1123)-back(1123),
    d20_8(1123)-back(1123),d20_9(1123)-back(1123),d20_10
    (1123)-back(1123)];
cc20 = [d20_1(1508)-back(1508),d20_2(1508)-back(1508),d20_3
    (1508)-back(1508),d20_4(1508)-back(1508),d20_5(1508)-back
    (1508), d20_6(1508)-back(1508),d20_7(1508)-back(1508),
```

```
d20_8(1508)-back(1508),d20_9(1508)-back(1508),d20_10
(1508)-back(1508)];
wv20 = [d20_1(3130)-back(3130),d20_2(3130)-back(3130),d20_3
(3130)-back(3130),d20_4(3130)-back(3130),d20_5(3130)-back
(3130), d20_6(3130)-back(3130),d20_7(3130)-back(3130),
d20_8(3130)-back(3130),d20_9(3130)-back(3130),d20_10
(3130)-back(3130)];
hy20 = [d20_1(3281)-back(3281),d20_2(3281)-back(3281),d20_3
(3281)-back(3281),d20_4(3281)-back(3281),d20_5(3281)-back
(3281), d20_6(3281)-back(3281),d20_7(3281)-back(3281),
d20_8(3281)-back(3281),d20_9(3281)-back(3281),d20_10
(3281)-back(3281)];
eq20 = [0.1, 0.2, 0.3, 0.4, 0.5, 0.6, 0.7, 0.8, 0.9, 1.0];

subplot(2, 2, 1)
plot(eq20, ch20)
title('CH peaks ve equivalence ratio')
xlabel('\phi');

subplot(2, 2, 2)
plot(eq20, cc20)
title('C2 peaks ve equivalence ratio')
xlabel('\phi');

subplot(2, 2, 3)
plot(eq20, wv20)
title('Water vapor peaks ve equivalence ratio')
xlabel('\phi');

subplot(2, 2, 4)
plot(eq20, hy20)
title('Hydroxyl peaks ve equivalence ratio')
xlabel('\phi');

%%
```

```
%%10
figure(10)
ch10 = [d10_2(1123)-back(1123),d10_3(1123)-back(1123),d10_4
    (1123)-back(1123),d10_5(1123)-back(1123)];
cc10 = [d10_2(1508)-back(1508),d10_3(1508)-back(1508),d10_4
    (1508)-back(1508),d10_5(1508)-back(1508)];
wv10 = [d10_2(3130)-back(3130),d10_3(3130)-back(3130),d10_4
    (3130)-back(3130),d10_5(3130)-back(3130)];
hy10 = [d10_2(3281)-back(3281),d10_3(3281)-back(3281),d10_4
    (3281)-back(3281),d10_5(3281)-back(3281)];
eq10 = [0.2, 0.3, 0.4, 0.5];

subplot(2, 2, 1)
plot(eq10, ch10)
title('CH peaks ve equivalence ratio')
xlabel('\phi');

subplot(2, 2, 2)
plot(eq10, cc10)
title('C2 peaks ve equivalence ratio')
xlabel('\phi');

subplot(2, 2, 3)
plot(eq10, wv10)
title('Water vapor peaks ve equivalence ratio')
xlabel('\phi');

subplot(2, 2, 4)
plot(eq10, hy10)
title('Hydroxyl peaks ve equivalence ratio')
xlabel('\phi');
```